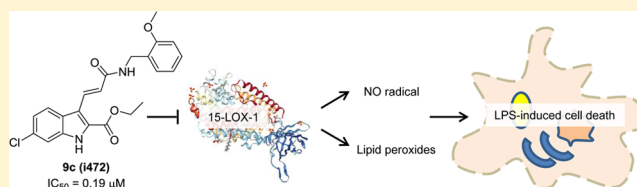


Novel 15-Lipoxygenase-1 Inhibitor Protects Macrophages from Lipopolysaccharide-Induced Cytotoxicity

Hao Guo,[†] Iris C. Verhoek,[†] Gerian G. H. Prins,[‡] Ramon van der Vlag,[§] Petra E. van der Wouden,[†] Ronald van Merkerk,[†] Wim J. Quax,[†] Peter Olinga,[‡] Anna K. H. Hirsch,^{§,||,⊥} and Frank J. Dekker^{*,†}[†]Department of Chemical and Pharmaceutical Biology and [‡]Department of Pharmaceutical Technology and Biopharmacy, Groningen Research Institute of Pharmacy (GRIP), University of Groningen, Antonius Deusinglaan 1, 9713 AV Groningen, The Netherlands[§]Department of Chemical Biology 2, Stratingh Institute for Chemistry, University of Groningen, Nijenborgh 7, 9747 AG Groningen, The Netherlands^{||}Helmholtz Institute for Pharmaceutical Research Saarland (HIPS)–Helmholtz Centre for Infection Research (HZI), Department of Drug Design and Optimization, Campus Building E8.1, 66123 Saarbrücken, Germany[⊥]Department of Pharmacy, Saarland University, 66123 Saarbrücken, Germany

Supporting Information

ABSTRACT: Various mechanisms for regulated cell death include the formation of oxidative mediators such as lipid peroxides and nitric oxide (NO). In this respect, 15-lipoxygenase-1 (15-LOX-1) is a key enzyme that catalyzes the formation of lipid peroxides. The actions of these peroxides are interconnected with nuclear factor- κ B signaling and NO production. Inhibition of 15-LOX-1 holds promise to interfere with regulated cell death in inflammatory conditions. In this study, a novel potent 15-LOX-1 inhibitor, **9c** (**i472**), was developed and structure–activity relationships were explored. In vitro, this inhibitor protected cells from lipopolysaccharide-induced cell death, inhibiting NO formation and lipid peroxidation. Thus, we provide a novel 15-LOX-1 inhibitor that inhibits cellular NO production and lipid peroxidation, which set the stage for further exploration of these mechanisms.



1. INTRODUCTION

Over recent years, an increasing number of mechanisms for regulated cell death have been identified and versatile roles in numerous diseases were proposed.¹ Cell death via a mechanism other than apoptosis leads to plasma membrane rupture and release of the cellular content, thus providing damage-associated molecular patterns that can induce an autoamplification loop of regulated cell death and inflammation. Such amplification loops are expected to play key roles in diseases such as acute lung injury and acute respiratory distress syndrome.² Understanding the underlying mechanisms to develop small-molecule inhibitors to interfere with cell death holds promise for therapeutic control of these disorders.

The discovery of multiple types of cell death provides new challenges to identify the molecular mechanisms involved. One mechanism of nonapoptotic cell death is pyroptosis in which macrophages die by excessive stimulation of Toll-like receptors and activation of the nuclear factor- κ B (NF- κ B) pathway by, for example, lipopolysaccharides (LPS).^{2–6} Normally, pyroptosis is a mechanism to protect multicellular organisms from invading pathogens, such as microbial infections. However, under pathogenic conditions, pyroptosis can be involved in the onset of chronic inflammation. Another mechanism for nonapoptotic cell death is ferroptosis, which is a process in which excessive levels of lipid peroxides cause cell death. It is anticipated that

lipoxygenases (LOXs) play key roles in ferroptosis by catalyzing lipid peroxidation.^{2,7} The identification of pyroptosis, ferroptosis, and other mechanisms for regulated cell death raises the question how these mechanisms can be exploited for drug discovery.

Although distinct mechanisms for regulated cell death were described, the mechanisms involved are often closely related and crosstalk exists. In this study, we aim to address the crosstalk between macrophage cell death upon LPS stimulation and the enzymatic activity of 15-lipoxygenase-1 (15-LOX-1) as a regulator of cellular lipid peroxidation (Figure 1).⁸ Activation of the NF- κ B pathway results in transcription of downstream genes, such as inducible nitric oxide synthase (iNOS), that plays a critical role in inflammatory responses.⁹ iNOS catalyzes the formation of NO radicals that play key roles in many physiological processes.¹⁰ On the other hand, excessive NO production can lead to the formation of reactive nitrogen species (RNOS), which induces cell death and tissue damage.¹¹

Reactive oxygen species (ROS) such as lipid peroxides have been shown to augment LPS-mediated NF- κ B activation and thus increase expression of NF- κ B target genes,^{8,12} which represents a mechanism of crosstalk between lipid peroxidation

Received: February 1, 2019

Published: April 9, 2019

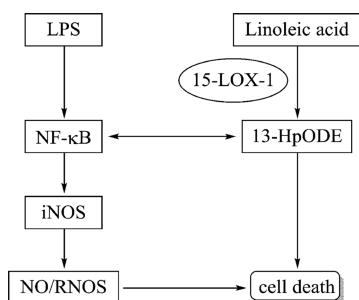


Figure 1. Several mechanisms of lipopolysaccharide (LPS) signaling in macrophages are connected to cell death. LPS-mediated activation of the NF- κ B pathway results in the overexpression of inducible nitric oxide synthase (iNOS). This leads to the production of nitric oxide (NO) and reactive nitrogen species (RNOS), which are involved in cell death. In the 15-LOX-1 pathway, 13-hydroperoxyoctadecadienoic acid (13-HpODE), the metabolite of 15-LOX-1 activity, can also induce cell death. Both mechanisms act in concert, and crosstalk exists.

and NF- κ B activation. 15-LOX-1 is a nonheme iron-containing enzyme producing lipid peroxides from polyunsaturated fatty acids, such as arachidonic acid (AA) and linoleic acid (LA).^{13–15} 15-LOX-1 oxidizes either AA, to form the corresponding 15-hydroxyeicosatetraenoic acid, or LA, to form the corresponding 13-hydroperoxyoctadecadienoic acid (13-HpODE).^{16,17} Apart from these hydroperoxy fatty acids, lipoxins are also derived from the 15-LOXs pathway and play a role as anti-inflammatory mediators.¹⁸ On the other hand, the 15-LOX metabolites eoxins are proposed to be a family of proinflammatory eicosanoids.¹⁹ Altogether, lipid peroxides can be converted further into distinct lipid signaling molecules that have key regulatory roles in immune responses^{20–22} and numerous diseases.²³ Importantly, if the production of lipid peroxides is not balanced by the cellular antioxidant system, this can result in ferroptotic cell death and in enhanced activation of the NF- κ B pathway, thus providing synergistic crosstalk between two mechanisms of regulated cell

death.²⁴ Thus, 15-LOX-1 is a key enzyme in oxidative stress and regulated cell death in numerous diseases.^{13,25,26}

For 15-LOX-1, roles have been described in diseases such as asthma,¹⁴ stroke,¹⁵ atherogenesis,² diabetes,^{16,17} cancer,^{20,21} Alzheimer's disease,^{22,23} and Parkinson's disease.²⁵ This triggered the interest in the development of 15-LOX-1 inhibitors for drug discovery. In an early phase, indole-based inhibitors, PD-146176, were identified as r-12/15-LOX inhibitors with a half-maximal inhibitory concentration (IC_{50}) value of 3.81 μ M (Figure 2).²⁷ This stimulated efforts to develop inhibitors with an indolyl core (Figure 2). More researchers reported the discovery of indole-based or indole-like 15-LOX-1 inhibitors, 371 and Haydi-4b (with IC_{50} values of 0.006 and 3.84 μ M, respectively).^{28,29} Our group previously discovered 15-LOX-1 inhibitor Eleftheriadis-14d, which also contains an indole core and demonstrates good potency (IC_{50} = 90 nM).³⁰ Furthermore, a 1,3-oxazole-based compound (ML351),³¹ a purine-based compound (Anders-6b),³² and pyrrole-based compound (21B10)³³ were identified as 15-LOX-1 inhibitors as well (Figure 1). These inhibitors proved to be effective in various disease models, thus indicating the potential of 15-LOX-1 inhibitors for drug discovery.

Complementary to development of inhibitors, efforts were made to engineer 15-LOX-1 substrates for detection of enzyme activity. We developed activity-based probe N144 as a chemical reporter for lipoxygenase activity in cell lysates and tissue samples.³⁴ Another study employed the omega-alkynyl fatty acid (aAA) to identify the intracellular targets of 12/15-LOX-generated lipid-derived electrophiles.³⁵ This sets the stage for the development of potent 15-LOX-1 inhibitors and to study their cellular activity.

In this study, we investigated novel substitutions of the indole core and investigated the structure–activity relationships (SARs) for 15-LOX-1 inhibition. For the most potent inhibitor, the effects on cellular 15-LOX-1 inhibition, the effects on formation of reactive oxygen species (ROS), and regulated cell

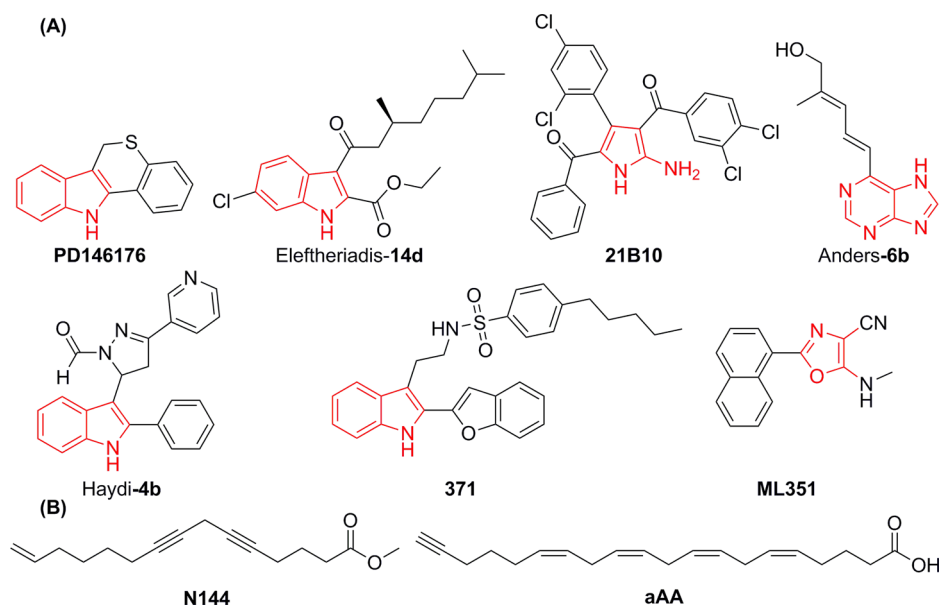
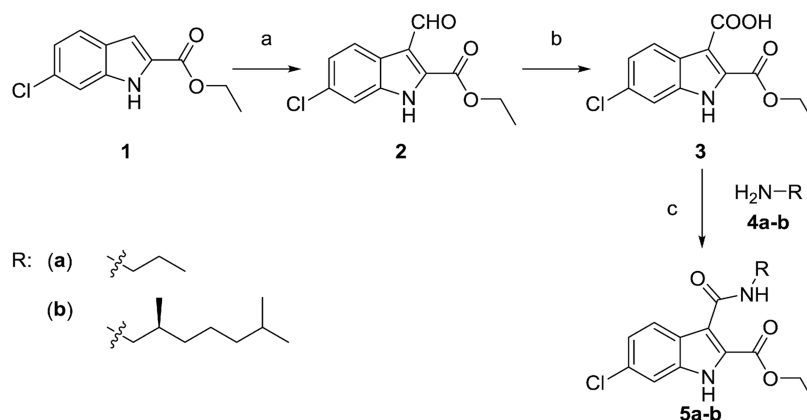
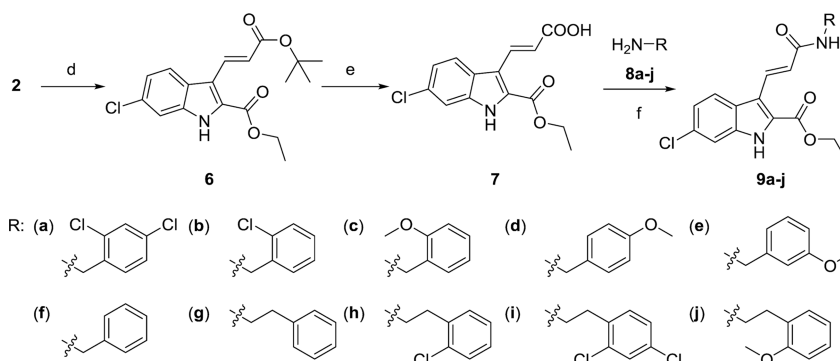


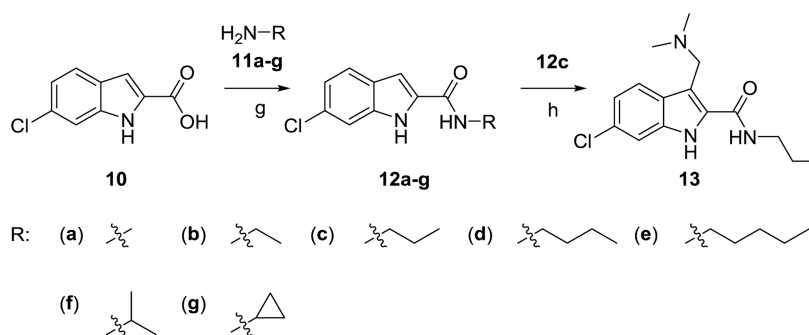
Figure 2. Examples of previously reported 15-LOX-1 inhibitors and chemical tools to study lipoxygenase activity. (A) Indole-based 15-LOX-1 inhibitor and inhibitors based on other nitrogen-containing heterocycles. (B) Substrate-based chemical tools to study lipoxygenase activity in cell-based systems.

Scheme 1. Synthetic Route to Compounds 5a and 5b^a

^aReagents and conditions: (a) POCl₃, dimethylformamide (DMF), 60 °C, 48 h; (b) NaClO₂, *t*-BuOH, 50 °C, 4 h; (c) amine (4a and 4b), EDCI, HOBT, Et₃N, dichloromethane (DCM), room temperature (r.t.), 4 h.

Scheme 2. Synthetic Route to Compounds 9a–j^a

^aReagents and conditions: (d) (*tert*-butoxycarbonylmethylene)triphenylphosphorane, EtOH, reflux, 2 h; (e) TFA, DCM, r.t., overnight; (f) amine (8a–j), EDCI, HOBT, Et₃N, DCM, r.t., 4 h.

Scheme 3. Synthetic Route to Compounds 12a–g and 13^a

^aReagents and conditions: (g) amine (11a–g), EDCI, HOBT, Et₃N, DCM, r.t., 4 h; (h) dimethylamine, formaldehyde, acetic acid, MeOH, reflux, 4 h.

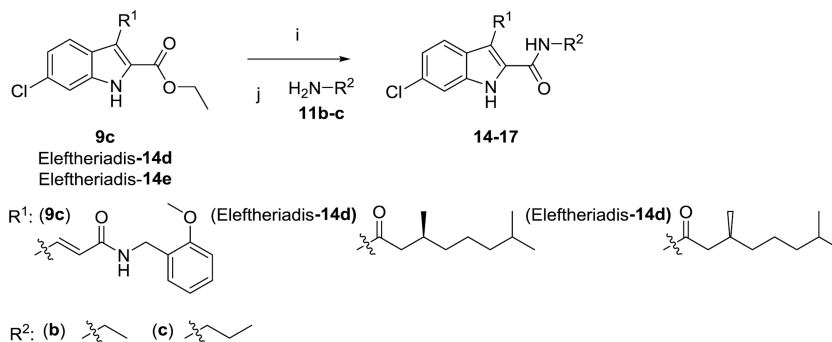
death were investigated on RAW 264.7 macrophages to provide insight into the cellular potency of this type of inhibitors.

2. RESULTS AND DISCUSSION

2.1. Chemistry. Scheme 1 presents the general methodology for the synthesis of compounds 5a and 5b. The synthesis started with the assembly of ethyl 6-chloro-1H-indole-2-carboxylate (1) and the corresponding aldehyde (2) using known literature procedures.^{30,36} Subsequently, the 2-formyl functionality of the aldehyde 2 was oxidized into its corresponding carboxylic acid

(3) via Pinnick oxidation using sodium chlorite (NaClO₂), giving a yield of 78%. Attempts to use KMnO₄ or Tollens' reagent did not provide the desired product. Finally, the amide bonds in products 5a and 5b were generated using 1-ethyl-3-(3-dimethylaminopropyl)carbodiimide (EDCI) and *N*-hydroxybenzotriazole (HOBT) as coupling reagents, giving yields of about 85%.

Compounds 9a–j were synthesized using procedures as shown in Scheme 2. As a first step, the 2-formyl functionality of aldehyde 2 was employed for the Wittig reaction with (*tert*-

Scheme 4. Synthetic Route to Compounds 14–17^a

^aReagents and conditions: (i) LiOH, THF, H₂O, 50 °C, 2 h; (j) EDCI, HOBt, Et₃N, DCM, r.t., 4 h.

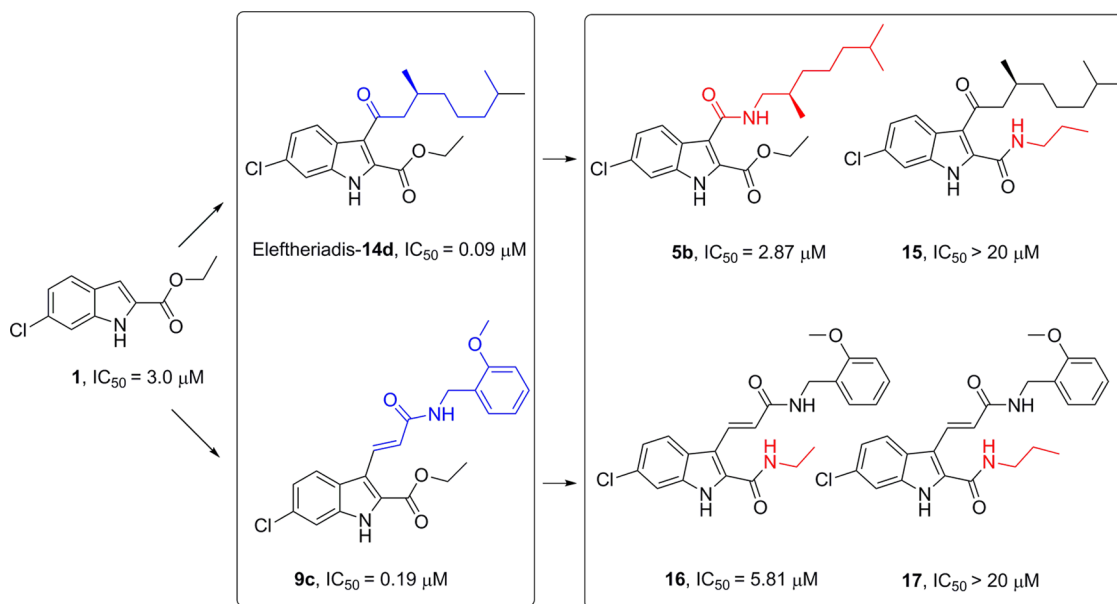


Figure 3. Systematic modifications of 15-LOX-1 inhibitor **1** as a core scaffold and the previously described inhibitor Eleftheriadis-14d³⁰ to provide the new inhibitors **5b**, **9c**, **15–17** and their IC₅₀ values for 15-LOX-1 inhibition.

butoxycarbonylmethylene)triphenylphosphorane to provide the α,β -unsaturated ester **6**. Initially, attempts were made to obtain compound **7** by refluxing aldehyde **2** with the Wittig reagent in toluene overnight. However, this provided compound **6** as a mixture of *E*- and *Z*-isomers (*E/Z* = approximately 9/1).³⁷ Changing the solvent from toluene to ethanol at 80 °C enabled the reaction to finish in 2 h with the *E*-alkene as the major product that could be isolated in a yield of 70% after purification. The *E*- and *Z*-isomer could be distinguished by their *J* values of 16.0 and 7.0 Hz, respectively. Finally, intermediate **7** was converted into the amides **9a–j** by removal of the *tert*-butyl protecting group using trifluoroacetic acid (TFA) treatment and subsequent coupling of the corresponding amines using 1-ethyl-3-(3-dimethylaminopropyl)carbodiimide (EDCI) and *N*-hydroxybenzotriazole (HOBt) as coupling reagents in yields between 80 and 90% over two steps.

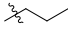
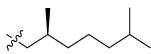
Products **12a–g** were produced starting from compound **10** as shown in Scheme 3. The carboxylic acid **10** was coupled to amines **11a–g** using EDCI and HOBt as coupling reagents, which gives the desired products in 80–90% yield. Afterward, compound **13** was obtained from compound **12c** using a Mannich reaction with dimethylamine, formaldehyde, and acetic acid to provide the desired product in a yield of 93%.

As shown in Scheme 4, compounds **14–17** were obtained from the corresponding 2-carboxy ethyl indoles (**9c**, Eleftheriadis-14d and Eleftheriadis-14e) over two steps in a similar way as for **12a–g** in a high yield (80–90%).

2.2. Structure–Activity Relationships. Inhibition of 15-LOX-1 enzyme activity was performed using an activity assay as described previously by us.^{30,33,38} The activity of 15-LOX-1 was monitored by measuring the conversion of LA into the UV-active 13-HpODE (λ_{max} 234 nm). This assay was used to determine IC₅₀ of each compound. SARs for binding to 15-LOX-1 were investigated starting from ethyl 6-chloro-1*H*-indole-2-carboxylate (**1**). We aimed to introduce structural modifications to replace the lipid chain at the 3-position and the ethylcarboxylate at the 2-position. Key structural modifications are shown in Figure 3 starting from previously identified inhibitors **1** and Eleftheriadis-14d.³⁰

The SAR of the previously identified inhibitor Eleftheriadis-14d was explored with respect to aliphatic acyl substitutions at the indole 3-position. To expand the SAR in novel directions, the carboxyl ethyl ester at the indole 3-position was replaced by an amide to gain metabolic stability. Both compounds **5a** and **5b** (Scheme 1 and Table 1) provided IC₅₀ values above 1 μM , which is much higher compared to that of the previously

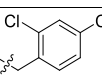
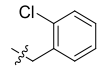
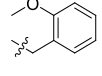
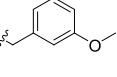
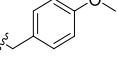
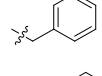
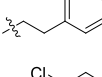
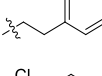
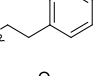
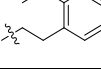
Table 1. IC₅₀ Values for 15-LOX-1 Inhibition by Amide-Substituted Indoles at the 3-Position (Analogues 5a and 5b)

Compound	R	IC ₅₀ (μM)
		[± SD (μM)]
5a		> 20
5b		2.87 ± 1.81

reported series of inhibitors with the carboxyl ethyl ester.³⁰ Apparently, replacement of the carbonyl at the indole 3-position for an amide is unfavorable for 15-LOX-1 inhibition.

The SAR at the indole 3-position was further explored by replacement of the carbonyl at the 3-position for a double bond using Wittig chemistry. Using this chemistry, we aimed to replace the aliphatic lipid chain in Eleftheriadis-14d for less flexible substituents. Thus, we investigated a series of *E*-alkenes as shown in Table 2. Clear SARs were observed for this series of compounds. Compound 9c (i472) proved to be the most potent 15-LOX-1 inhibitor with an IC₅₀ value of 0.19 μM. Comparison of inhibitor 9c (i472) to inhibitor 9f indicates that the *ortho*-methoxy substitution on benzyl provides a 10-fold gain in potency compared to that of a nonsubstituted benzyl. Importantly, the IC₅₀ values decrease if the methoxy group is

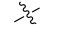
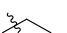
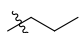
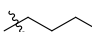
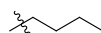
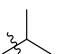

Table 2. IC₅₀ Values against 15-LOX-1 with Different Variations in R (Analogues 9a–j)

Compound	R	IC ₅₀ (μM)
		[± SD (μM)]
9a		2.95 ± 1.28
9b (i44)		0.74 ± 0.22
9c (i472)		0.19 ± 0.03
9d		0.40 ± 0.01
9e		0.75 ± 0.31
9f		2.43 ± 0.96
9g		>20
9h		1.29 ± 0.42
9i		0.19 ± 0.05
9j		0.27 ± 0.01

moved from the *ortho* to the *meta* or *para* position on benzyl 9d and 9e. Extending the benzyl to an ethylphenyl group in inhibitors 9g–j did not improve their potencies either. Taken together, the 2-methoxybenzyl group in 9c (i472) provides the most potent inhibitor in this series.

To further explore the SAR of previously identified inhibitor Eleftheriadis-14d, variations were made at the indolyl 2-position. Toward this aim, the ester group was replaced with various amides to provide inhibitors 12a–g, as shown in Table 3.

Table 3. IC₅₀ Values against 15-LOX-1 with Different Variations in the Amide Tail (Analogues 12a–g)

Compound	R	IC ₅₀ (μM)
		[± SD (μM)]
12a		9.38 ± 2.63
12b		6.88 ± 2.32
12c		4.09 ± 1.11
12d		13.02 ± 2.73
12e		10.94 ± 2.21
12f		9.82 ± 1.41
12g		>20

The results indicate that amide substitution provides inhibitors with potencies in the micromolar range. However, the SAR for modifications with methyl, ethyl, *n*-propyl, *n*-butyl, *n*-pentyl, and branched alkyl groups proved to be relatively flat with potency differences of no more than 2–3-fold. Remarkably, cyclopropyl substitution in 12g turns out to be inactive (IC₅₀ > 20 μM). Taken together, the investigated series of amide-substituted indoles did not provide improved potency and the most potent inhibitor in this series is compound 12c with a propyl substitution.

As a next step, we combined ethyl- or propyl-substituted amides at the indole 2-position with substitutions at the 3-position to provide inhibitors 14–17, as shown in Table 4. Unfortunately, the combination of both modifications provided inhibitors with low potency. Apparently, the more polar amide bond is not well tolerated for enzyme inhibition and combination of modifications at the 2- and 3-position caused a greatly reduced potency. Inhibitor 13 also showed a complete loss in potency against 15-LOX-1. Taken together, we concluded that inhibitor 9c (i472) has the highest potency of this series and that the IC₅₀ value is in the same range as for the previously identified inhibitor Eleftheriadis-14d.

2.3. Docking 15-LOX-1. To understand the observed SAR key inhibitors were docked in the 15-LOX-1 active site. In this study, docking was performed using Discovery Studio (Dassault Systèmes) version 2018. Moreover, the rabbit reticulocyte 15-LOX-1 crystal structure (Protein Data Bank (PDB) ID: 1LOX) was used for docking because of its high sequence similarity in the active site.³⁹ In this crystal structure, the ligand in the crystal structure was removed and the center of the binding sphere was set at the same position. Based on this position, CDocker, a

Table 4. IC₅₀ Values against 15-LOX-1 with Different Variations in R¹ and R² (Analogues 13–18)

Compound	R ¹	R ²	IC ₅₀ (μM) [± SD (μM)]
13			>20
14			>20
15			>20
16			5.81 ± 1.18
17			>20

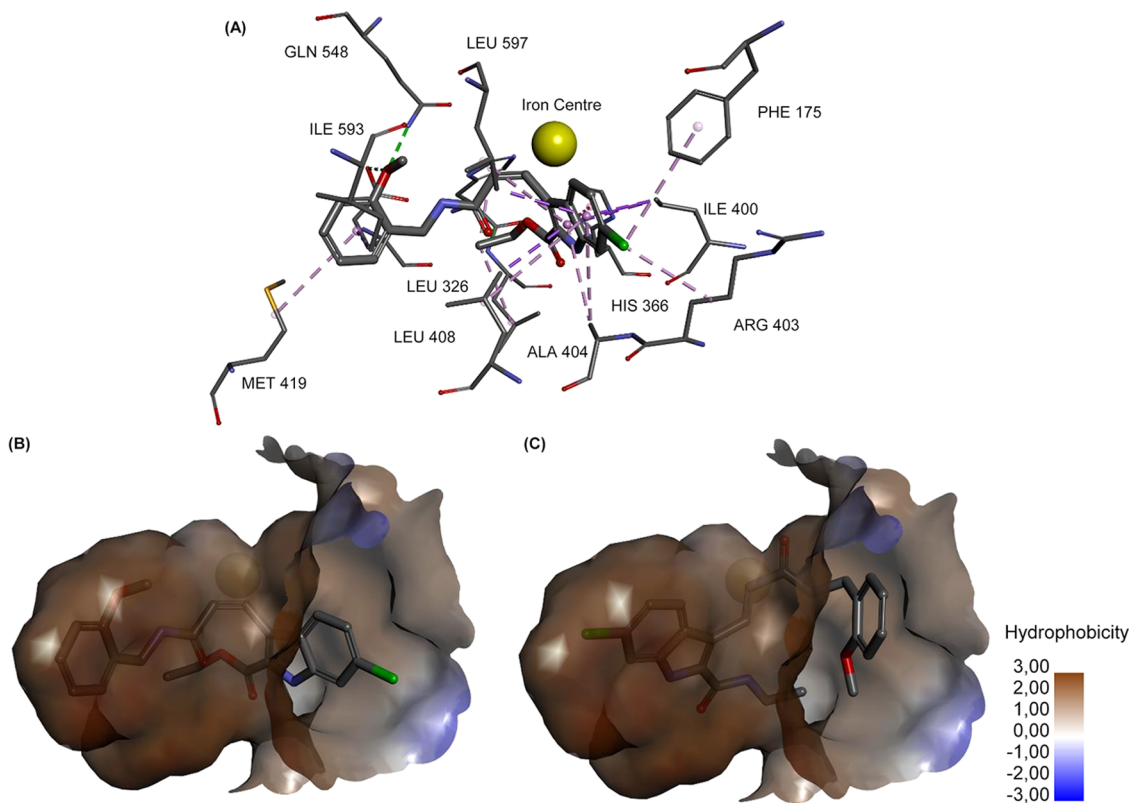


Figure 4. Molecular modeling of selected compounds in the active site of 15-LOX-1 (PDB ID: 1LOX). The surface in the pocket is colored based on the relative hydrophobicity: brown for hydrophobic and blue for hydrophilic areas. (A) Interactions of compound **9c** (**i472**) with the active site of the enzyme. (B) Preferred orientation of compound **9c** (**i472**) in the active site of the enzyme. (C) Preferred orientation of compound **16** in the active site of the enzyme that is inverted compared to **9c** (**i472**).

CHARMm-based method, was used and resulted in ten highest-ranked poses for all selected inhibitors.

Based on the observed SAR, the most potent inhibitor **9c** (**i472**) was docked and compared to **9f** (lacking the methoxy group) and **16** (in which the ester is replaced for an amide). In both cases, the potency decreased by at least 10-fold. The docking model suggested several interactions between the active

site of 15-LOX-1 and **9c** (**i472**), as shown in [Figure 4A](#). Upon comparison of the docking of **9c** (**i472**) and **9f**, the 2-methoxy group on the benzyl functionality provides two hydrogen bonds with GLN 548 and ILE 593, respectively ([Figure 4A](#)). This may provide an explanation for the 10-fold potency difference between **9c** (**i472**) and **9f**. In addition, because of the hydrophobic character of 15-LOX-1, except from the edge of

the active site, the majority of the pocket is hydrophobic, as shown in brown in Figure 4B,C. The hydrophilic sites are shown in blue. Docking of compound **16**, in which an amide replaces the carboxy ethyl ester at the indole 2-position, shows a positionally inverted orientation compared to **9c** (**i472**) and **9f** (Figures 4C and S1C). Apparently, the amide with an additional hydrogen bond donor does not fit at the same position as the ester in **9c** (**i472**). This change in orientation upon docking is also in line with the observed drop in potency for **16** compared to **9c** (**i472**) and **9f**.

2.4. Physicochemical Properties of Inhibitor **9c** (**i472**).

The α,β -unsaturated amide functionality in **9c** (**i472**) is, as a Michael acceptor, reactive toward conjugate addition by nucleophiles, such as thiols. To monitor this reactivity, the UV spectrum of **9c** (**i472**) was recorded upon incubation with 2-mercaptoethanol at pH 7.4. No changes in the UV spectrum were observed, which indicates that the chromophore, including the α,β -unsaturated system, did not change (Figure S2), thus indicating a reasonable stability of compound **9c** (**i472**) toward nucleophilic substitution. This stability might be attributed to the conjugation of the α,β -unsaturated double bond with the aromatic indole core.

Inhibitor **9c** (**i472**) has a calculated Log *P* (ChemDraw Professional version 12.0) of 4.7, which is more than 2 orders of magnitude lower compared to the previously identified inhibitor Eleftheriadis-**14d** (cLog *P* = 6.9), whereas both inhibitors have molecular weights around 400 g/mol. Considering the physicochemical properties, the newly identified inhibitor **9c** (**i472**) has fewer rotatable bonds and a cLog *P* that is more favorable for cellular permeability compared to the previously identified inhibitor Eleftheriadis-**14d**.

2.5. LOX Inhibitory Potency of **9c (**i472**) in Cells by Activity-Based Labeling.** As a next step in the characterization of inhibitor **9c** (**i472**), the inhibition of cellular LOX activity was investigated. Toward this aim, we employed a method for activity-based labeling of LOX activity in cell-based systems that we developed recently.³⁴ In this method, a covalent inhibitor of lipoxygenase activity is equipped with a terminal alkene for bioorthogonal labeling with biotin using the oxidative Heck reaction.⁴⁰ Here, we employed this method to estimate the inhibition of cellular lipoxygenase activity by inhibitor **9c** (**i472**) in RAW 264.7 macrophages. Inhibitor-treated and nontreated cell lysates were exposed to covalent inhibitor **N144** (Figure 2) for 2 min, and subsequently, the samples were subjected to the oxidative Heck reaction to link a biotinylated phenylboronic acid for detection. In parallel to the labeling, the same samples were subjected to staining for β -actin as a loading control and antibody-based detection of the amount of 15-LOX-1. Representative blots are shown in Figure 5. We observed a decreased intensity for the band for activity-based lipoxygenase labeling as detected by streptavidin-horseradish peroxidase (HRP). For comparison, the bands normalized with the β -actin antibody and the 15-LOX antibody were included as well, which show comparable intensities. Quantifications of the bands from three independent experiments are shown in Figure 6. From these results, we conclude that 15-LOX-1 inhibitor **9c** (**i472**) is able to inhibit the activity of cellular lipoxygenases.

2.6. Protection of RAW 264.7 Macrophages from LPS-Induced Cytotoxicity. After identifying compound **9c** (**i472**) as a potent inhibitor for recombinant expressed 15-LOX-1 and cellular LOX activity, we moved on to investigate the potency of this compound in cell-based studies. As the insight into the mechanism, we presume that 15-LOX-1 inhibitors inhibit the

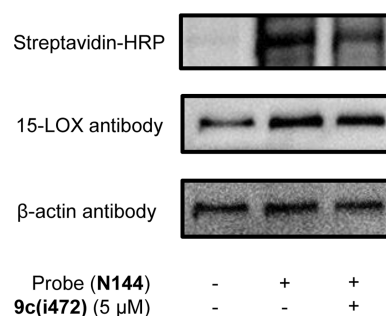


Figure 5. Detection of the effect of inhibitor **9c** (**i472**) on the activity of 15-LOX-1 by an activity-based probe. Labeling was performed on cell lysis of RAW 264.7 cells. Positive control (with probe and without inhibitor), negative control (without probe or inhibitor), and incubation of **9c** (**i472**) were performed with the 15-LOX antibody, β -actin antibody, and streptavidin-HRP ($n = 3$).

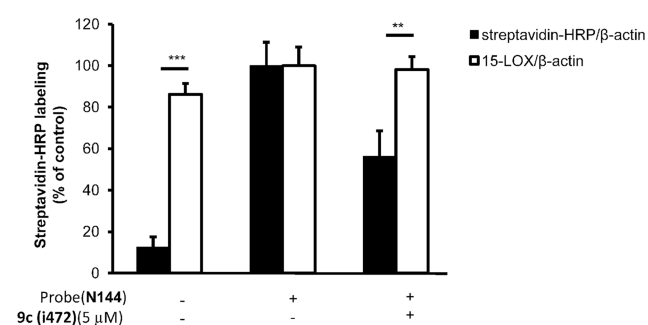


Figure 6. Quantification of Western blots for detection and analysis of activity-based labeling: The values are measured by integrating the gray values by ImageJ 1.44. The integrated gray values of streptavidin-HRP and 15-LOX are normalized to β -actin, respectively. All of the values were expressed as mean \pm standard error of the mean (SEM). The results were normalized by three independent experiments ($n = 3$). * $p < 0.05$, ** $p < 0.005$, and *** $p < 0.001$ compared to control by the two-tailed test.

formation of lipid peroxides in cells, thereby preventing ferroptotic cell death. Additionally, we expect this mechanism to have crosstalk with the NF- κ B pathway. Activation of this pathway can also lead to cell death. To test this hypothesis, we employed a model in which we stimulated RAW 264.7 macrophages with LPS to cause cell death, as reported previously.³ This study reported an LD₅₀ of 89.5 μ g/mL for LPS-induced cell death in macrophages. In our experiments, 40% inhibition of cell viability was obtained at 100 μ g/mL (Figure S3). Subsequently, as shown in Figure 7, we employed an LPS concentration of 100 μ g/mL and investigated the protection from cell death by treatment with lipoxygenase inhibitors. The 5-LOX inhibitor **Zileuton** and the previously identified 15-LOX-1 inhibitor Eleftheriadis-**14d** comparably improved the viability of LPS-treated RAW 264.7 macrophages. In addition, inhibitor **9c** (**i472**) showed stronger, dose-dependent effects with a 20% viability increase at 5 μ M. Thus, these data demonstrated that inhibiting 15-LOX-1 by compound **9c** (**i472**) can protect RAW 264.7 macrophages from LPS-induced cell death.

2.7. NF- κ B Activity Determination. To gain further insight into the mechanism of protection for LPS-induced cell death, we investigated the effect of inhibitor **9c** (**i472**) on NF- κ B activity using an NF- κ B reporter assay on RAW-Blue macrophages (modified RAW 264.7 macrophages). These RAW-Blue

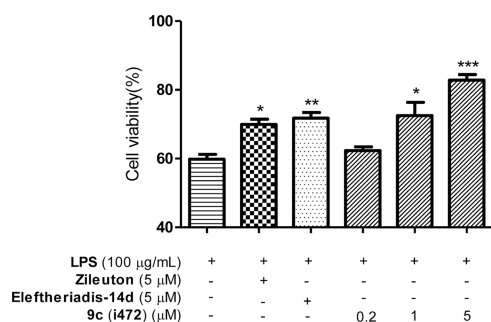


Figure 7. Inhibitor **9c** (**i472**) protects RAW 264.7 macrophages from LPS-induced cytotoxicity. RAW 264.7 macrophages were treated with lipopolysaccharides (LPSs) (100 µg/mL) and **9c** (**i472**) together for 24 h. Then, the cell viability was determined by a 3-(4,5-dimethylthiazol-2-yl)-5-(3-carboxymethoxyphenyl)-2-(4-sulfophenyl)-2H-tetrazolium (MTS) assay ($n = 3-13$). All of the values were expressed as mean \pm SEM. * $p < 0.05$, ** $p < 0.005$, and *** $p < 0.001$ compared to positive control by the two-tailed test that is only with the treatment of LPS (100 µg/mL) for 48 h.

macrophages can stably express a secreted embryonic alkaline phosphatase (SEAP) gene that is inducible by NF- κ B and AP-1 transcription factors. Previous evidence demonstrated that the product of 15-LOX-1 and 13-HpODE can increase NF- κ B activation but has no effect on AP-1.⁸ The cells were stimulated with LPS, interferon γ (IFN γ), and inhibitor **9c** (**i472**).⁴¹ This provided significant but not complete inhibition of NF- κ B transcriptional activation upon LPS/IFN γ stimulation (Figure 8). These results are in line with the anticipated crosstalk between 15-LOX-1 inhibition and NF- κ B signaling.

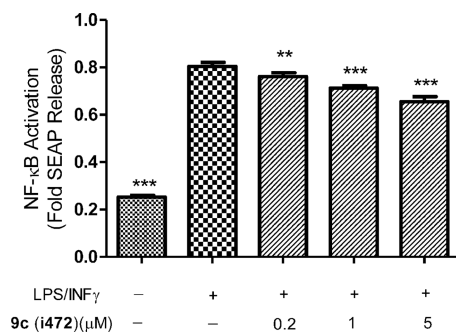


Figure 8. Inhibitor **9c** (**i472**) reduces NF- κ B activity. RAW-Blue macrophages were pretreated with inhibitor **9c** (**i472**) at 0.2, 1, and 5 µM for 20 h, after which inflammatory lipopolysaccharide (LPS) and interferon γ (IFN γ) stimuli (10 ng/mL of each) were given for another 4 h in continued presence of inhibitor **9c**. All of the values were expressed as mean \pm SEM ($n = 8-16$). * $p < 0.05$, ** $p < 0.005$, and *** $p < 0.001$ compared to positive control that is treated with LPS and IFN γ by the two-tailed test.

2.8. Gene Expression. Subsequently, we turned our attention to the influence of 15-LOX-1 inhibition by **9c** (**i472**) on the gene expression of NF- κ B-related gene iNOS (Figure 9). As a model, we used RAW 264.7 macrophages that were activated by LPS and IFN γ (10 ng/mL of each).⁴² The gene expression of iNOS was downregulated by approximately 50% at 5 µM. This finding is in line with but more pronounced than the observed decrease in NF- κ B transcriptional activity (Figure 8).

2.9. Quantification of Nitric Oxide (NO) Production. Gene transcription of iNOS is connected to NO production,

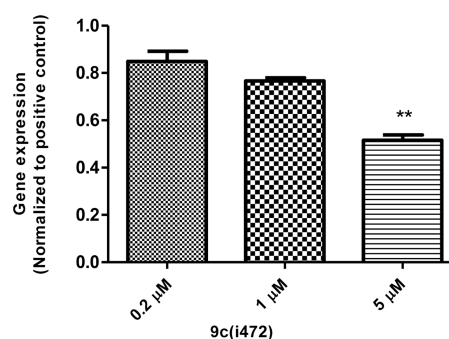


Figure 9. Effect of inhibition of 15-LOX-1 by **9c** (**i472**) on iNOS in RAW 264.7 cells: Lipopolysaccharide (LPS)/interferon γ (IFN γ) (10 ng/mL of each)-stimulated cells were normalized to the positive control. All experimental groups were treated with compound **9c** (**i472**) at 0.2, 1, and 5 µM for 20 h and stimulated with LPS/IFN γ for another 4 h ($n = 3-4$). All of the values were expressed as mean \pm SEM. * $p < 0.05$, ** $p < 0.005$, and *** $p < 0.001$ compared to the LPS/IFN γ -treated positive control group by the two-tailed test.

which plays an important role in the regulation of immune response and apoptosis. In our study, we compared the inhibitory effects of **9c** (**i472**) on the ratio of total nitrate to nitrite in RAW 264.7 macrophages (Figure 10). We

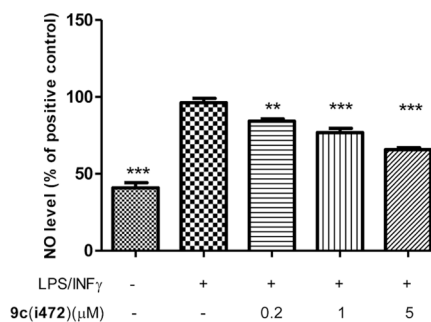


Figure 10. Dose-dependent effect of **9c** (**i472**) on the expression of total nitrate/nitrite in RAW 264.7 cells: Lipopolysaccharide (LPS)/interferon γ (IFN γ) (10 ng/mL of each)-stimulated cells were corrected to 100% as positive control. All experimental groups were treated with compound **9c** (**i472**) at 0.2, 1, and 5 µM for 20 h and stimulated with LPS/IFN γ for another 4 h ($n = 3$). All of the values were expressed as mean \pm SEM. * $p < 0.05$, ** $p < 0.005$, and *** $p < 0.001$ compared to the LPS/IFN γ -treated control group by the two-tailed test.

demonstrated that **9c** (**i472**) as a 15-LOX-1 inhibitor provided dose-dependent inhibition of NO production, which is consistent with the results of reduced activity of NF- κ B and the gene expression of iNOS. The observations that 15-LOX inhibition inhibits NF- κ B reporter gene activity, iNOS expression, and NO levels are in line with the idea that there is crosstalk between 15-LOX-1 activity and cell death via activity of the NF- κ B pathway and NO production.

2.10. Lipid Peroxidation. Oxidative stress can cause a series of toxic effects through the production of lipid peroxides that play a role in cell death.⁴³ The effect of lipoxygenase inhibitor **9c** (**i472**) on lipid peroxidation in RAW 264.7 cells was investigated using the fluorescent dye dipyrrometheneboron difluoride (BODIPY) 581/591 C₁₁ and fluorescence-activated cell sorting (FACS).⁴⁴ As shown in Figure 11, 15-LOX inhibitor PD-146176 and **9c** (**i472**) revealed comparable effects that both of them significantly attenuated the boost of lipid peroxides

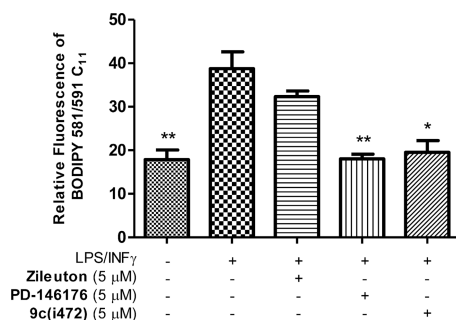


Figure 11. Analysis of lipid peroxidation using BODIPY 581/591 C11 staining and FACS analysis. Cells were treated with lipopolysaccharide (LPS)/interferon γ (IFN γ) (10 ng/mL of each) and PD-146176 (5 μ M), Zileuton (5 μ M), or 9c (i472) (5 μ M). Results are represented as mean \pm SEM ($n = 3$). * $p < 0.05$, ** $p < 0.005$, and *** $p < 0.001$ compared to the LPS/IFN γ -treated control group by the two-tailed test.

at 5 μ M after the treatment of LPS/IFN γ (10 ng/mL of each). This result could be attributed to loss of 15-LOX products, such as 13-HpODE. Furthermore, compared to the 5-LOX inhibitor, Zileuton, both 15-LOX-1 inhibitors showed a more pronounced effect on lipid peroxidation, fitting the result of LPS-induced cell death assay that the 15-LOX-1 inhibitor has a better rescue effect. Although 15-LOX-1 is not the only pathway that can trigger lipid peroxide formation, these results indicate that inhibition of 15-LOX-1 has a strong influence on lipid peroxidation in this model system.

3. CONCLUSIONS

In this study, compound 9c (i472) was developed as a potent 15-LOX-1 inhibitor with a novel substituent pattern ($IC_{50} = 0.19 \mu$ M) and its SARs were explored. Using activity-based labeling, we demonstrated that inhibitor 9c (i472) was able to inhibit cellular lipoxygenases. Further characterization of this compound demonstrated that it was able to protect RAW 264.7 macrophages from LPS-induced cell death. We explored the influence of inhibitor 9c (i472) on different pathways of cell death. We investigated NF- κ B activation, iNOS expression, and NO formation as a line of events that can trigger cell death. Treatment with inhibitor 9c (i472) enabled downregulation of the NF- κ B transcriptional activity in a reporter gene assay. Furthermore, we demonstrated that iNOS gene expression and the levels of NO in RAW 264.7 macrophages decreased significantly upon 9c (i472) treatment. As a direct effect of inhibiting lipoxygenase activity, we investigated inhibition of cellular lipid peroxidation upon 9c (i472) treatment, for which we observed a clear reduction back to baseline levels. Having explored both mechanisms, we can conclude that inhibitor 9c (i472) influences both NO production and lipid peroxidation, potentially via a crosstalk mechanism. Thus, we conclude that we provide a novel 15-LOX-1 inhibitor 9c (i472) with cellular activity that inhibits the formation of oxidative mediators, such as NO and lipid peroxides, that are connected to different mechanisms for cell death.

4. EXPERIMENTAL SECTION

4.1. General. All reagents, solvents, and catalysts were purchased from commercial sources (Acros Organics, Sigma-Aldrich, and abcr GmbH, Netherlands) and used without purification. Reactions that required exclusion of oxygen or water were performed in oven-dried flasks under nitrogen atmosphere. Reactions were monitored by thin-

layer chromatography (TLC) on TLC precoated (250 μ m) silica gel 60 F₂₅₄ aluminum foil (EMD Chemicals Inc.). Visualization was achieved using UV light. Alternatively, non-UV-active compounds were detected after staining with potassium permanganate. Flash column chromatography was performed on silica gel (32–63 μ m, 60 Å pore size). ¹H NMR (500 MHz) and ¹³C NMR (126 MHz) spectra were recorded with a Bruker Avance four-channel NMR spectrometer with a TXI probe. Chemical shifts (δ) are reported in ppm. Abbreviations are as follows: singlet (s), doublet (d), triplet (t), quartet (q), and multiplet (m). Fourier transform mass spectrometry and electrospray ionization were performed on an Applied Biosystems/SCIEX API 3000-triple quadrupole mass spectrometer. High-performance liquid chromatography (HPLC) analysis was performed for confirming purity with a Shimadzu LC-10AT HPLC, with a Shimadzu SP-M10A ELSD detector, and with a Shimadzu SPD-M10A photodiode array detector. Analytical HPLC was performed using a Kinetex C18 column (150 mm \times 4.6 mm, 5 μ m) with 5–95% MeCN gradient in H₂O as a mobile phase, confirming purity $\geq 95\%$. Retention time (RT) of HPLC was also reported.

4.2. Synthesis and Characterization. **4.2.1. Ethyl 6-Chloro-3-formyl-1H-indole-2-carboxylate (2).** To a solution of POCl₃ (0.30 mL, 3.2 mmol, 1.2 equiv) in DMF (6.0 mL) stirred at 0 $^{\circ}$ C for 0.5 h, 1 (0.60 g, 2.7 mmol) was added, and the reaction mixture was heated to 50 $^{\circ}$ C for 46 h. After completion, the reaction mixture was slowly poured into a mixture of crushed ice and H₂O (300 mL). The product was obtained by filtration of the resulting suspension. The residue was washed with acetonitrile and dried at r.t., giving the title intermediate 2 as a yellow solid in a yield of 83% (0.55 g, 2.2 mmol). The NMR spectra were the same as reported previously.³⁶

4.2.2. 6-Chloro-2-(ethoxycarbonyl)-1H-indole-3-carboxylic Acid (3). To a solution of 2 (0.10 g, 0.39 mmol) and NaClO₂ (71 mg, 0.78 mmol) was added 5.0 mL of *t*-BuOH at 50 $^{\circ}$ C for 4 h. After reaction completion, the mixture was concentrated and H₂O (50 mL) was added, followed by extraction with EtOAc (3 \times 15 mL). The organic phases were collected and evaporated, giving a white crude product without further purification in 82% yield.

4.2.3. General Synthetic Procedure 1: Amide Bond Formation. The respective carboxylic acid (1.0 equiv) was added to a mixture of HOBt (0.40 equiv), EDCI (2.0 equiv), and Et₃N (1.0 equiv) in CH₂Cl₂ (20 mL) at room temperature for 30 min. After stirring, the respective amine (1.5 equiv) was added to this reaction mixture, which was subsequently stirred at room temperature for 4 h. Then, the reaction mixture was washed with 1.0 M aqueous HCl (5.0 mL), sat. aqueous NaHCO₃ (5.0 mL), and brine (5.0 mL); dried over MgSO₄; filtered; and concentrated under reduced pressure. The crude product was purified by column chromatography and eluted with 20% ethyl acetate in DCM as a solvent to obtain a white solid product with a general yield from 70 to 80%.

4.2.4. Ethyl 6-Chloro-3-(propylcarbamoyl)-1H-indole-2-carboxylate (5a). The product was obtained using general procedure 1 starting from carboxylate 3 and propylamine. The product was obtained as a yellow solid in 86% yield. ¹H NMR (500 MHz, dimethyl sulfoxide (DMSO)-*d*₆) δ 12.96 (s, 1H), 8.92 (t, $J = 5.5$ Hz, 1H), 8.57 (d, $J = 2.5$ Hz, 1H), 7.87 (d, $J = 8.5$ Hz, 1H), 7.35 (dd, $J = 8.5, 2.5$ Hz, 1H), 4.31 (q, $J = 7.0$ Hz, 2H), 3.26–3.23 (m, 2H), 1.59–1.52 (m, 2H), 1.32 (t, $J = 7.0$ Hz, 3H), 0.91 (t, $J = 7.0$ Hz, 3H). ¹³C NMR (126 MHz, DMSO-*d*₆) δ 167.37, 160.16, 154.97, 139.38, 136.90, 130.43, 130.37, 124.08, 120.02, 119.90, 63.31, 41.49, 22.49, 14.26, 11.88. High-resolution mass spectrometry (HRMS), calcd for C₁₅H₁₈ClO₂N₃ [M + H]⁺: 309.1000, found 309.1002. HPLC: purity 96%, retention time 17.7 min.

4.2.5. Ethyl (R)-6-Chloro-3-((2,6-dimethylheptyl)carbamoyl)-1H-indole-2-carboxylate (5b). The product was obtained using general procedure 1 starting from carboxylate 3. The product was obtained as a yellow solid in 82% yield. ¹H NMR (500 MHz, CDCl₃) δ 10.75 (s, 1H), 9.40 (s, 1H), 8.43 (d, $J = 8.5$ Hz, 1H), 7.50 (d, $J = 2.0$ Hz, 1H), 7.36 (dd, $J = 8.5, 2.0$ Hz, 1H), 5.75 (s, 1H), 4.56 (q, $J = 7.0$ Hz, 2H), 3.25–3.06 (m, 1H), 1.54 (m, 1H), 1.51 (t, $J = 5.0$ Hz, 3H), 1.36–1.15 (m, 8H), 0.96 (d, $J = 6.0$ Hz, 3H), 0.93 (d, $J = 6.0$ Hz, 3H). ¹³C NMR (126 MHz, DMSO-*d*₆) δ 166.71, 160.13, 154.91, 139.28, 136.81, 131.58, 130.40, 124.03, 120.33, 119.92, 63.29, 45.55, 38.70, 36.64, 36.34, 27.81, 24.04,

22.87, 20.86, 14.26, 14.18. HRMS, calcd for $C_{21}H_{30}ClN_2O_3$ $[M + H]^+$: 393.1939, found 393.1938. HPLC: purity 99%, retention time 14.3 min.

4.2.6. Ethyl (E)-3-(3-(tert-Butoxy)-3-oxoprop-1-en-1-yl)-6-chloro-1H-indole-2-carboxylate (6). 2 (0.10 g, 0.39 mmol), (tert-butoxycarbonylmethylene)triphenylphosphorane (0.17 g, 0.50 mmol), and EtOH (10 mL) were mixed under an atmosphere of nitrogen in an oven-dried flask. The mixture was heated at reflux for 2 h. Then, the solvent was evaporated under reduced pressure. The product was purified by column chromatography and eluted with 20% ethyl acetate in petroleum as a solvent, and a yellow solid product was obtained in 84% yield. The NMR spectra were the same as reported previously.⁴⁵

4.2.7. (E)-3-(6-Chloro-2-(ethoxycarbonyl)-1H-indol-3-yl)acrylic Acid (7). 6 (0.50 g, 1.7 mmol) was dissolved in DCM (1 mL). Then, trifluoroacetic acid (1.0 mL, 2.0 mmol) was added and the mixture was stirred at 0 °C for 2 h. After evaporation of the solvent, the crude product did not need further purification. The NMR spectra were the same as reported previously.⁴⁵

4.2.8. Ethyl (E)-6-Chloro-3-(3-((2,4-dichlorobenzyl)amino)-3-oxoprop-1-en-1-yl)-1H-indole-2-carboxylate (9a). The product was obtained using general procedure 1 starting from 7. The product was obtained as a white solid in 89% yield. ¹H NMR (500 MHz, DMSO-*d*₆) δ 12.31 (s, 1H), 8.63 (t, *J* = 6.0 Hz, 1H), 8.34 (d, *J* = 16.0 Hz, 1H), 8.06 (d, *J* = 8.5 Hz, 1H), 7.65 (d, *J* = 2.0 Hz, 1H), 7.55 (d, *J* = 2.0 Hz, 1H), 7.48–7.43 (m, 2H), 7.28 (dd, *J* = 8.5, 2.0 Hz, 1H), 7.24 (d, *J* = 16.0 Hz, 1H), 4.48 (d, *J* = 6.0 Hz, 2H), 4.41 (q, *J* = 7.0 Hz, 2H), 1.39 (t, *J* = 7.0 Hz, 3H). ¹³C NMR (126 MHz, DMSO-*d*₆) δ 166.16, 161.20, 137.57, 136.10, 133.64, 132.81, 132.02, 131.12, 130.47, 129.09, 127.88, 127.66, 123.97, 123.71, 122.58, 122.37, 117.17, 113.10, 105.90, 61.59, 14.69. HRMS, calcd for $C_{21}H_{18}Cl_2N_2O_3$ $[M + H]^+$: 451.0378, found 451.0377. HPLC: purity 95%, retention time 19.2 min.

4.2.9. Ethyl (E)-6-Chloro-3-(3-((2-chlorobenzyl)amino)-3-oxoprop-1-en-1-yl)-1H-indole-2-carboxylate (9b). The product was obtained using general procedure 1 starting from 7. The product was obtained as a white solid in 89% yield. ¹H NMR (500 MHz, DMSO-*d*₆) δ 12.32 (s, 1H), 8.59 (t, *J* = 5.5 Hz, 1H), 8.34 (d, *J* = 16.0 Hz, 1H), 8.07 (d, *J* = 6.0 Hz, 1H), 8.55 (d, *J* = 2.0 Hz, 1H), 7.48 (dd, *J* = 7.0, 2.0 Hz, 1H), 7.43 (dd, *J* = 7.0, 2.0 Hz, 1H), 7.35 (m, 2H), 7.28 (dd, *J* = 7.0, 2.0 Hz, 1H), 7.03 (d, *J* = 16 Hz, 1H), 4.50 (d, *J* = 6.0 Hz, 2H), 4.42 (q, *J* = 6.0 Hz, 2H), 1.39 (t, *J* = 6.0 Hz, 3H). ¹³C NMR (126 MHz, DMSO-*d*₆) δ 171.36, 166.33, 141.59, 140.42, 134.65, 134.42, 133.89, 133.21, 131.51, 130.11, 129.20, 127.64, 126.67, 125.90, 122.91, 122.09, 117.00, 99.98, 65.72, 34.31, 19.24. HRMS, calcd for $C_{21}H_{19}O_3N_2Cl_2$ $[M + H]^+$: 417.0767, found 417.0767. HPLC: purity 96%, retention time 19.2 min.

4.2.10. Ethyl (E)-6-Chloro-3-(3-((2-methoxybenzyl)amino)-3-oxoprop-1-en-1-yl)-1H-indole-2-carboxylate (9c). The product was obtained using general procedure 1 starting from 7. The product was obtained as a white solid in 79% yield. ¹H NMR (500 MHz, DMSO-*d*₆) δ 12.28 (s, 1H), 8.39 (t, *J* = 5.5 Hz, 1H), 8.31 (d, *J* = 16.0 Hz, 1H), 8.08 (d, *J* = 9.0 Hz, 1H), 7.54 (dd, *J* = 7.0, 2.0 Hz, 1H), 7.42–7.29 (m, 3H), 7.03 (s, 1H), 7.01 (d, *J* = 7.0 Hz, 1H), 6.94 (td, *J* = 7.0, 2.0 Hz, 1H), 4.43–4.38 (m, 4H), 3.83 (s, 3H), 1.39 (t, *J* = 7.0 Hz, 3H). ¹³C NMR (126 MHz, DMSO-*d*₆) δ 165.97, 161.25, 157.28, 141.43, 137.57, 131.43, 130.44, 128.78, 127.53, 125.63, 124.96, 124.11, 123.96, 122.30, 120.66, 117.37, 113.09, 111.04, 61.57, 55.78, 38.81, 14.73. HRMS, calcd for $C_{22}H_{22}ClN_2O_4$ $[M + H]^+$: 413.1263, found 413.1261. HPLC: purity 96%, retention time 18.9 min.

4.2.11. Ethyl (E)-6-Chloro-3-(3-((3-methoxybenzyl)amino)-3-oxoprop-1-en-1-yl)-1H-indole-2-carboxylate (9d). The product was obtained using general procedure 1 starting from 7. The product was obtained as a white solid in 91% yield. ¹H NMR (500 MHz, DMSO-*d*₆) δ 12.30 (s, 1H), 8.55 (t, *J* = 6.0 Hz, 1H), 8.34 (d, *J* = 16.0 Hz, 1H), 8.05 (d, *J* = 8.5 Hz, 1H), 7.55 (d, *J* = 2.0 Hz, 1H), 7.29–7.25 (m, 2H), 6.94 (d, *J* = 16.0 Hz, 1H), 6.91 (m, 2H), 6.85 (dd, *J* = 7.0, 2.0 Hz, 1H), 4.44–4.40 (m, 4H), 3.74 (s, 3H), 1.39 (t, *J* = 7.0 Hz, 3H). ¹³C NMR (126 MHz, DMSO-*d*₆) δ 165.92, 161.24, 159.82, 141.43, 137.57, 131.69, 130.45, 129.68, 127.53, 125.63, 124.96, 123.97, 123.05, 122.34, 120.13, 117.30, 113.66, 112.71, 61.58, 55.54, 42.84, 14.75. HRMS, calcd for $C_{22}H_{22}ClN_2O_4$ $[M + H]^+$: 413.1263, found 413.1262. HPLC: purity 96%, retention time 14.4 min.

4.2.12. Ethyl (E)-6-Chloro-3-(3-((4-methoxybenzyl)amino)-3-oxoprop-1-en-1-yl)-1H-indole-2-carboxylate (9e). The product was obtained using general procedure 1 starting from 7. The product was obtained as a white solid in 84% yield. ¹H NMR (500 MHz, DMSO-*d*₆) δ 12.29 (s, 1H), 8.49 (t, *J* = 6.0 Hz, 1H), 8.34 (d, *J* = 16.0 Hz, 1H), 8.04 (d, *J* = 6.0 Hz, 1H), 7.54 (d, *J* = 2.0 Hz, 1H), 7.26 (m, 3H), 6.97–6.91 (m, 3H), 4.43 (q, *J* = 6.0 Hz, 2H), 4.35 (d, *J* = 6.0 Hz, 2H), 3.74 (s, 3H), 1.39 (t, *J* = 6.0 Hz, 3H). ¹³C NMR (126 MHz, DMSO-*d*₆) δ 165.77, 161.24, 158.78, 137.56, 131.76, 131.52, 130.43 (2×), 129.35, 127.48, 123.95, 123.72, 123.22, 122.32, 117.33, 114.27, 114.21, 113.11, 61.58, 55.52, 42.35, 14.67. HRMS, calcd for $C_{22}H_{22}ClN_2O_4$ $[M + H]^+$: 413.1263, found 413.1262. HPLC: purity 95%, retention time 14.4 min.

4.2.13. Ethyl (E)-3-(3-(Benzylamino)-3-oxoprop-1-en-1-yl)-6-chloro-1H-indole-2-carboxylate (9f). The product was obtained using general procedure 1 starting from 7. The product was obtained as a white solid in 88% yield. ¹H NMR (500 MHz, DMSO-*d*₆) δ 12.30 (s, 1H), 8.57 (t, *J* = 6.0 Hz, 1H), 8.33 (d, *J* = 16.0 Hz, 1H), 8.05 (d, *J* = 6.0 Hz, 1H), 7.55 (d, *J* = 2.0 Hz, 1H), 7.38–7.25 (m, 6H), 6.67 (d, *J* = 16.0 Hz, 1H), 4.44–4.40 (m, 4H), 1.38 (t, *J* = 6.0 Hz, 3H). ¹³C NMR (126 MHz, DMSO-*d*₆) δ 165.91, 161.24, 139.86, 137.56, 131.68, 131.62, 130.44, 128.86 (2×), 127.98, 127.52, 127.38, 123.96, 123.77, 123.08, 122.34, 117.30, 113.02, 61.59, 42.88, 14.76. HRMS, calcd for $C_{21}H_{20}ClN_2O_3$ $[M + H]^+$: 383.1157, found 383.1158. HPLC: purity 98%, retention time 7.1 min.

4.2.14. Ethyl (E)-6-Chloro-3-(3-oxo-3-(phenethylamino)prop-1-en-1-yl)-1H-indole-2-carboxylate (9g). The product was obtained using general procedure 1 starting from 7. The product was obtained as a white solid in 76% yield. ¹H NMR (500 MHz, DMSO-*d*₆) δ 12.28 (s, 1H), 8.29 (d, *J* = 16.0 Hz, 1H), 8.19 (t, *J* = 6.0 Hz, 1H), 8.02 (d, *J* = 7.5 Hz, 1H), 7.54 (d, *J* = 2.0 Hz, 1H), 7.34–7.21 (m, 6H), 6.90 (d, *J* = 16.0 Hz, 1H), 4.42 (q, *J* = 6.0 Hz, 2H), 4.45 (q, *J* = 6.0 Hz, 2H), 2.81 (t, *J* = 6.0 Hz, 2H), 1.38 (t, *J* = 6.0 Hz, 3H). ¹³C NMR (126 MHz, DMSO-*d*₆) δ 165.90, 161.24, 144.40, 139.98, 137.58, 137.13, 131.26, 130.41 (2×), 129.09, 128.82, 126.57, 123.97, 123.70, 123.26, 122.28, 117.34, 113.06, 61.55, 39.77, 35.74, 14.71. HRMS, calcd for $C_{22}H_{22}ClN_2O_3$ $[M + H]^+$: 397.1313, found 397.1311. HPLC: purity 96%, retention time 14.5 min.

4.2.15. Ethyl (E)-6-Chloro-3-(3-((2-chlorophenethyl)amino)-3-oxoprop-1-en-1-yl)-1H-indole-2-carboxylate (9h). The product was obtained using general procedure 1 starting from 7. The product was obtained as a white solid in 90% yield. ¹H NMR (500 MHz, DMSO-*d*₆) δ 12.28 (s, 1H), 8.28 (d, *J* = 16.0 Hz, 1H), 8.24 (t, *J* = 6.0 Hz, 1H), 8.02 (d, *J* = 9.0 Hz, 1H), 7.55 (d, *J* = 2.0 Hz, 1H), 7.46 (dd, *J* = 8.0, 2.0 Hz, 1H), 7.38 (dd, *J* = 8.0, 2.0 Hz, 1H), 7.33–7.26 (m, 3H), 6.87 (d, *J* = 16.0 Hz, 1H), 4.42 (q, *J* = 7.0 Hz, 2H), 3.45 (q, *J* = 7.0 Hz, 2H), 2.95 (t, *J* = 7.0 Hz, 2H), 1.40 (t, *J* = 7.0 Hz, 3H). ¹³C NMR (126 MHz, DMSO-*d*₆) δ 166.01, 161.53, 137.21, 136.78, 133.50, 131.21, 129.66, 129.44, 128.67, 128.58, 127.78, 127.68, 125.82, 125.02, 123.80, 120.88, 118.46, 112.26, 61.13, 38.63, 33.14, 14.71. HRMS, calcd for $C_{22}H_{21}O_3N_2Cl_2$ $[M + H]^+$: 431.0924, found 431.0924. HPLC: purity 95%, retention time 14.2 min.

4.2.16. Ethyl (E)-6-Chloro-3-(3-((2,4-dichlorophenethyl)amino)-3-oxoprop-1-en-1-yl)-1H-indole-2-carboxylate (9i). The product was obtained using general procedure 1 starting from 7. The product was obtained as a white solid in 89% yield. ¹H NMR (500 MHz, DMSO-*d*₆) δ 12.29 (s, 1H), 8.28 (d, *J* = 16.0 Hz, 1H), 8.22 (t, *J* = 6.0 Hz, 1H), 8.01 (d, *J* = 9.0 Hz, 1H), 7.62 (d, *J* = 2.0 Hz, 1H), 7.55 (d, *J* = 2.0 Hz, 1H), 7.40 (m, 2H), 7.28 (m, 1H), 6.85 (d, *J* = 16.0 Hz, 1H), 4.42 (q, *J* = 7.0 Hz, 2H), 3.48 (q, *J* = 7.0 Hz, 2H), 2.91 (t, *J* = 7.0 Hz, 2H), 1.36 (t, *J* = 7.0 Hz, 3H). ¹³C NMR (126 MHz, DMSO-*d*₆) δ 165.97, 161.22, 137.55, 136.49, 134.57, 132.79, 132.21, 131.38, 130.44, 129.12, 127.86, 127.49, 123.97, 123.65, 123.13, 122.32, 117.29, 113.07, 61.56, 38.69, 32.96, 14.70. HRMS, calcd for $C_{22}H_{20}O_3N_2Cl_3$ $[M + H]^+$: 465.0534, found 465.0534. HPLC: purity 95%, retention time 18.2 min.

4.2.17. Ethyl (E)-6-Chloro-3-(3-((2-methoxyphenethyl)amino)-3-oxoprop-1-en-1-yl)-1H-indole-2-carboxylate (9j). The product was obtained using general procedure 1 starting from 7. The product was obtained as a white solid in 81% yield. ¹H NMR (500 MHz, DMSO-*d*₆) δ 12.27 (s, 1H), 8.27 (d, *J* = 16.0 Hz, 1H), 8.17 (t, *J* = 5.5 Hz, 1H), 8.02 (d, *J* = 8.5 Hz, 1H), 7.54 (d, *J* = 2.0 Hz, 1H), 7.27 (dd, *J* = 8.0, 2.0 Hz, 1H), 7.22 (m, 1H), 7.18 (dd, *J* = 7.0, 2.0 Hz, 1H), 6.99 (d, *J* = 16.0 Hz,

1H), 6.89 (m, 2H), 4.42 (q, $J = 7.0$ Hz, 2H), 3.81 (s, 3H), 3.32 (q, $J = 7.0$ Hz, 2H), 2.78 (t, $J = 7.0$ Hz, 2H), 1.39 (t, $J = 7.0$ Hz, 3H). ^{13}C NMR (126 MHz, DMSO- d_6) δ 165.84, 161.25, 157.71, 137.56, 131.17, 130.43, 128.09, 127.61, 127.41, 123.96, 123.75, 123.68, 123.41, 122.31, 117.38, 113.11, 113.00, 111.12, 61.56, 55.80, 55.71, 30.50, 14.75. HRMS, calcd for $\text{C}_{23}\text{H}_{24}\text{O}_4\text{N}_2\text{Cl}$ [$\text{M} + \text{H}$] $^+$: 427.1419, found 427.1418. HPLC: purity 96%, retention time 17.2 min.

4.2.18. 6-Chloro-N-methyl-1H-indole-2-carboxamide (12a). The product was obtained using general procedure 1 starting from **10**. The product was obtained as a light brown solid in 92% yield. ^1H NMR (500 MHz, DMSO- d_6) δ 11.72 (s, 1H), 8.53 (d, $J = 5.0$ Hz, 1H), 7.65 (d, $J = 8.5$ Hz, 1H), 7.43 (d, $J = 2.0$ Hz, 1H), 7.09 (d, $J = 2.0$ Hz, 1H), 7.05 (dd, $J = 8.5$, 2.0 Hz, 1H), 2.82 (d, $J = 4.5$ Hz, 3H). ^{13}C NMR (126 MHz, CDCl_3) δ 172.08, 162.03, 143.15, 135.19, 125.34, 125.14, 122.83, 113.47, 99.98, 35.69. HRMS, calcd for $\text{C}_{10}\text{H}_{10}\text{ClN}_2\text{O}$ [$\text{M} + \text{H}$] $^+$: 209.0476, found 209.0475. HPLC: purity 95%, retention time 18.5 min.

4.2.19. 6-Chloro-N-ethyl-1H-indole-2-carboxamide (12b). The product was obtained using general procedure 1 starting from **10**. The product was obtained as a light brown solid in 94% yield. ^1H NMR (500 MHz, DMSO- d_6) δ 11.70 (s, 1H), 8.65 (t, $J = 6.0$ Hz, 1H), 7.69 (d, $J = 8.5$ Hz, 1H), 7.43 (d, $J = 2.0$ Hz, 1H), 7.12 (d, $J = 2.0$ Hz, 1H), 7.06 (dd, $J = 8.5$, 2.0 Hz, 1H), 3.31 (m, 2H), 1.15 (t, $J = 7.5$ Hz, 3H). ^{13}C NMR (126 MHz, DMSO- d_6) δ 160.95, 137.05, 133.44, 128.15, 126.35, 123.55, 120.62, 112.17, 102.68, 34.13, 15.38. HRMS, calcd for $\text{C}_{11}\text{H}_{12}\text{ON}_2\text{Cl}$ [$\text{M} + \text{H}$] $^+$: 223.0633, found 223.0633. HPLC: purity 98%, retention time 10.8 min.

4.2.20. 6-Chloro-N-propyl-1H-indole-2-carboxamide (12c). The product was obtained using general procedure 1 starting from **10**. The product was obtained as a light brown solid in 91% yield. ^1H NMR (500 MHz, DMSO- d_6) δ 11.70 (s, 1H), 8.56 (t, $J = 5.5$ Hz, 1H), 7.64 (d, $J = 8.5$ Hz, 1H), 7.45 (d, $J = 2.0$ Hz, 1H), 7.15 (d, $J = 2.0$ Hz, 1H), 7.05 (dd, $J = 8.5$, 2.0 Hz, 1H), 3.25 (q, $J = 7.0$ Hz, 2H), 1.55 (q, $J = 7.5$ Hz, 2H), 0.91 (d, $J = 2.0$ Hz, 1H). ^{13}C NMR (126 MHz, DMSO- d_6) δ 161.14, 137.07, 133.42, 128.18, 126.36, 123.54, 120.57, 112.18, 102.75, 41.06, 22.97, 11.94. HRMS, calcd for $\text{C}_{12}\text{H}_{14}\text{ON}_2\text{Cl}$ [$\text{M} + \text{H}$] $^+$: 237.0789, found 237.0789. HPLC: purity 95%, retention time 14.5 min.

4.2.21. N-Butyl-6-chloro-1H-indole-2-carboxamide (12d). The product was obtained using general procedure 1 starting from **10**. The product was obtained as a light brown solid in 90% yield. ^1H NMR (500 MHz, DMSO- d_6) δ 11.96 (s, 1H), 7.45 (t, $J = 6.0$ Hz, 1H), 6.64 (d, $J = 8.5$ Hz, 1H), 7.43 (d, $J = 2.0$ Hz, 1H), 7.14 (d, $J = 2.0$ Hz, 1H), 7.20 (dd, $J = 8.5$, 2.0 Hz, 1H), 3.32 (q, $J = 7.5$ Hz, 2H), 1.57–1.53 (m, 2H), 1.39–1.34 (m, 2H), 0.90 (t, $J = 7.5$ Hz, 3H). ^{13}C NMR (126 MHz, DMSO- d_6) δ 161.07, 137.05, 133.42, 128.15, 126.36, 123.57, 120.59, 112.13, 102.70, 38.93, 31.79, 20.10, 14.20. HRMS, calcd for $\text{C}_{13}\text{H}_{16}\text{ClN}_2\text{O}$ [$\text{M} + \text{H}$] $^+$: 251.0946, found 251.0947. HPLC: purity 99%, retention time 14.5 min.

4.2.22. 6-Chloro-N-pentyl-1H-indole-2-carboxamide (12e). The product was obtained using general procedure 1 starting from **10**. The product was obtained as a light brown solid in 91% yield. ^1H NMR (500 MHz, DMSO- d_6) δ 11.69 (s, 1H), 7.51 (t, $J = 6.0$ Hz, 1H), 6.66 (d, $J = 8.5$ Hz, 1H), 7.43 (s, 1H), 7.14 (m, 1H), 7.03 (dd, $J = 8.5$, 2.0 Hz, 1H), 3.30 (q, $J = 7.5$ Hz, 2H), 1.57–1.53 (m, 2H), 1.24–1.20 (m, 4H), 0.92 (t, $J = 7.5$ Hz, 3H). ^{13}C NMR (126 MHz, DMSO- d_6) δ 161.05, 137.05, 133.42, 128.15, 126.35, 123.54, 120.55, 112.15, 102.72, 39.21, 29.36, 29.15, 22.36, 14.44. HRMS, calcd for $\text{C}_{14}\text{H}_{18}\text{ClN}_2\text{O}$ [$\text{M} + \text{H}$] $^+$: 265.1102, found 265.1103. HPLC: purity 99%, retention time 14.3 min.

4.2.23. 6-Chloro-N-isopropyl-1H-indole-2-carboxamide (12f). The product was obtained using general procedure 1 starting from **10**. The product was obtained as a light brown solid in 84% yield. ^1H NMR (500 MHz, DMSO- d_6) δ 11.67 (s, 1H), 8.30 (d, $J = 8.0$ Hz, 1H), 6.66 (d, $J = 8.5$ Hz, 1H), 7.43 (s, 1H), 7.14 (d, $J = 2.0$ Hz, 1H), 7.03 (dd, $J = 8.5$, 2.0 Hz, 1H), 4.17–4.09 (m, 1H), 1.20 (d, $J = 6.5$ Hz, 6H). ^{13}C NMR (126 MHz, DMSO- d_6) δ 160.28, 137.04, 133.50, 128.14, 126.33, 123.46, 120.56, 112.10, 102.88, 41.24, 41.14, 22.87. HRMS, calcd for $\text{C}_{12}\text{H}_{14}\text{ON}_2\text{Cl}$ [$\text{M} + \text{H}$] $^+$: 237.0789, found 237.0789. HPLC: purity 99%, retention time 10.8 min.

4.2.24. 6-Chloro-N-cyclopropyl-1H-indole-2-carboxamide (12g). The product was obtained using general procedure 1 starting from **10**.

The product was obtained as a light brown solid in 91% yield. ^1H NMR (500 MHz, DMSO- d_6) δ 11.70 (s, 1H), 8.54 (d, $J = 2.0$ Hz, 1H), 6.66 (d, $J = 8.5$ Hz, 1H), 7.43 (d, $J = 2.0$ Hz, 1H), 7.12 (d, $J = 2.0$ Hz, 1H), 7.06 (dd, $J = 8.5$, 2.5 Hz, 1H), 2.90–2.83 (m, 1H), 0.75–0.71 (m, 2H), 0.61–0.55 (m, 2H). ^{13}C NMR (126 MHz, DMSO- d_6) δ 162.36, 137.09, 133.14, 128.24, 126.32, 123.54, 120.63, 112.16, 103.01, 23.12 (2 \times), 6.30. HRMS, calcd for $\text{C}_{12}\text{H}_{12}\text{ON}_2\text{Cl}$ [$\text{M} + \text{H}$] $^+$: 235.0633, found 235.0632. HPLC: purity 97%, retention time 11.8 min.

4.2.25. 6-Chloro-3-((dimethylamino)methyl)-N-propyl-1H-indole-2-carboxamide (13). 6-Chloro-N-propyl-1H-indole-2-carboxamide (**12c**) (50 mg, 0.20 mmol), dimethylamine (9.5 mg, 0.20 mmol), paraformaldehyde (6.5 mg, 0.20 mmol), and 0.20 mL of acetic acid were dissolved in 10 mL of MeOH. The reaction mixture was refluxed for 4 h. After completion, the product was purified by column chromatography and eluted with 10% ethyl acetate in petroleum ether as a solvent to obtain a white solid product with 91% yield. ^1H NMR (500 MHz, DMSO- d_6) δ 11.75 (s, 1H), 10.53 (t, $J = 2.0$ Hz, 1H), 7.71 (d, $J = 8.5$ Hz, 1H), 7.43 (d, $J = 2.0$ Hz, 1H), 7.07 (dd, $J = 8.5$, 2.0 Hz, 1H), 3.69 (s, 2H), 3.29 (q, $J = 6.5$ Hz, 2H), 2.24 (s, 6H), 1.71–1.66 (m, 2H), 1.04 (t, $J = 7.0$ Hz, 3H). ^{13}C NMR (126 MHz, DMSO- d_6) δ 161.68, 135.54, 132.22, 128.27, 127.28, 121.36, 120.42, 112.11, 112.05, 52.57, 44.00, 43.97, 41.30, 22.75, 12.00. HRMS, calcd for $\text{C}_{15}\text{H}_{21}\text{ON}_3\text{Cl}$ [$\text{M} + \text{H}$] $^+$: 294.1368, found 294.1367. HPLC: purity 99%, retention time 13.9 min.

4.2.26. General Synthetic Procedure 2: Hydrolysis Reaction. The ester (1.0 equiv) was dissolved in THF (15 mL) while stirring. Then, a solution of lithium hydroxide trihydrate (3.0 equiv) in demiwater (15 mL) was added and the mixture was stirred at 50 $^\circ\text{C}$ for 2 h. Subsequently, the aqueous layer was extracted with EtOAc (3 \times 15 mL). The combined organic layers were washed with brine, dried over MgSO_4 , filtered, and concentrated under reduced pressure. The crude product **11** was used without further purification.

4.2.27. (R)-6-Chloro-3-(3,7-dimethyloctanoyl)-N-propyl-1H-indole-2-carboxamide (14). The product was obtained using general procedures 1 and 2 starting from compounds Eleftheriaidis-**14d** and **12c**. The product was obtained as a light brown solid in 65% yield over two steps. ^1H NMR (500 MHz, CDCl_3) δ 11.83 (s, 1H), 11.45 (t, $J = 2.0$ Hz, 1H), 7.88 (d, $J = 8.5$ Hz, 1H), 7.33 (d, $J = 2.0$ Hz, 1H), 7.31 (dd, $J = 8.5$, 2.5 Hz), 3.62 (q, $J = 6.5$ Hz, 2H), 3.06 (m, 2H), 2.28 (m, 1H), 1.83 (m, 2H), 1.56 (m, 1H), 1.42 (m, 2H), 1.33 (m, 2H), 1.22 (m, 2H), 1.12 (t, $J = 7.5$ Hz, 3H), 1.04 (d, $J = 7.5$ Hz, 3H), 0.89 (d, $J = 7.5$ Hz, 6H). ^{13}C NMR (126 MHz, CDCl_3) δ 199.61, 159.84, 136.61, 135.02, 130.45, 125.26, 123.66, 123.16, 115.54, 113.22, 51.18, 42.02, 39.08, 37.33, 29.61, 27.92, 24.79, 22.69, 22.62, 22.56, 20.01, 11.66. HRMS, calcd for $\text{C}_{22}\text{H}_{32}\text{O}_2\text{N}_2\text{Cl}$ [$\text{M} + \text{H}$] $^+$: 391.2147, found 391.2148. HPLC: purity 97%, retention time 21.4 min.

4.2.28. (S)-6-Chloro-3-(3,7-dimethyloctanoyl)-N-propyl-1H-indole-2-carboxamide (15). The product was obtained using general procedures 1 and 2 starting from compounds Eleftheriaidis-**14e** and **12c**. The product was obtained as a light brown solid in 55% yield over two steps. ^1H NMR (500 MHz, CDCl_3) δ 11.63 (s, 1H), 11.41 (t, $J = 2.0$ Hz, 1H), 7.88 (d, $J = 8.5$ Hz, 1H), 7.71 (d, $J = 2.0$ Hz, 1H), 7.31 (dd, $J = 8.5$, 2.5 Hz), 3.60 (q, $J = 7.0$ Hz, 2H), 3.19–2.96 (m, 2H), 2.30–2.25 (m, 1H), 1.85–1.78 (m, 2H), 1.60–1.52 (m, 1H), 1.46–1.16 (m, 6H), 1.12 (t, $J = 7.5$ Hz, 3H), 1.04 (d, $J = 6.5$ Hz, 3H), 0.90 (d, $J = 6.5$ Hz, 6H). ^{13}C NMR (126 MHz, CDCl_3) δ 199.60, 159.81, 136.62, 134.97, 130.46, 125.27, 123.66, 123.17, 115.53, 113.18, 51.18, 42.00, 39.08, 37.32, 29.60, 27.92, 24.79, 22.69, 22.62, 22.56, 20.00, 11.66. HRMS, calcd for $\text{C}_{22}\text{H}_{32}\text{O}_2\text{N}_2\text{Cl}$ [$\text{M} + \text{H}$] $^+$: 391.2147, found 391.2149. HPLC: purity 99%, retention time 22.9 min.

4.2.29. (E)-6-Chloro-N-ethyl-3-(3-((2-methoxybenzyl)amino)-3-oxoprop-1-en-1-yl)-1H-indole-2-carboxamide (16). The product was obtained using general procedures 1 and 2 starting from compounds **9c** and **11b**. The product was obtained as a white solid in 62% yield over two steps. ^1H NMR (500 MHz, DMSO- d_6) δ 12.01 (s, 1H), 8.47 (t, $J = 6.0$ Hz, 1H), 8.31 (t, $J = 6.0$ Hz, 1H), 8.19 (d, $J = 9.0$ Hz, 1H), 8.02 (d, $J = 7.5$ Hz, 1H), 7.50 (s, 1H), 7.25 (m, 3H), 7.04 (d, $J = 7.5$ Hz, 1H), 6.92 (t, $J = 7.5$ Hz, 1H), 6.89 (d, $J = 9.0$ Hz, 1H), 4.38 (d, $J = 6.0$ Hz, 2H), 3.84 (s, 3H), 3.33 (m, 2H), 1.19 (t, $J = 6.0$ Hz, 3H). ^{13}C NMR (126 MHz, DMSO- d_6) δ 166.34, 161.31, 157.29, 136.87, 134.45,

132.09, 129.02, 128.73, 127.32, 124.16, 123.14, 121.79, 120.79, 120.63, 113.16, 112.59, 111.05, 55.85, 37.93, 34.56, 31.15, 15.04. HRMS, calcd for $C_{22}H_{23}ClN_3O_3$ $[M + H]^+$: 412.4122, found 412.4123. HPLC: purity 96%, retention time 13.8 min.

4.2.30. (E)-6-Chloro-3-(3-((2-methoxybenzyl)amino)-3-oxoprop-1-en-1-yl)-N-propyl-1H-indole-2-carboxamide (17). The product was obtained using general procedures 1 and 2 starting from compounds **9c** and **11c**. The product was obtained as a white solid in 62% yield over two steps. 1H NMR (500 MHz, DMSO- d_6) δ 12.03 (s, 1H), 8.47 (t, J = 5.5 Hz, 1H), 8.29 (t, J = 5.5 Hz, 1H), 8.07 (d, J = 16.0 Hz, 1H), 8.01 (d, J = 9.0 Hz, 1H), 7.52 (d, J = 2.0 Hz, 1H), 7.23 (m, 3H), 7.20 (dd, J = 7.5, 2.0 Hz, 1H), 6.94 (td, J = 6.5, 2.0 Hz, 1H), 6.90 (d, J = 16.0 Hz, 1H), 4.38 (d, J = 6.0 Hz, 2H), 3.86 (s, 3H), 3.28 (q, J = 6.0 Hz, 2H), 1.68 (m, 2H), 0.95 (t, J = 6.0 Hz, 3H). ^{13}C NMR (126 MHz, DMSO- d_6) δ 166.32, 161.45, 157.26, 136.87, 134.57, 132.07, 128.98, 128.69, 128.66, 127.30, 124.13, 123.12, 121.77, 120.73, 120.62, 113.06, 112.58, 111.03, 55.84, 41.44, 37.92, 22.72, 12.01. HRMS, calcd for $C_{23}H_{25}ClN_3O_3$ $[M + H]^+$: 426.1579, found 426.1580. HPLC: purity 96%, retention time 13.8 min.

4.3. Human 15-LOX-1 Enzyme Inhibition Studies. The 15-LOX-1 enzyme was expressed and purified as described before.⁴⁶ Furthermore, the 15-LOX-1 enzyme activity studies were done using procedures previously described by our group as well.³⁰ 15-LOX-1 activity was determined by the conversion of linoleic acid to hydroperoxy-(9Z,11E)-octadecadienoic acid (λ_{max} of 234 nm) in a 96-well plate. The conversion rate was followed by UV absorbance at 234 nm. The conversion rate was evaluated at the linear part of the plot, and the substrate depletion covers the first 16 min. The optimum concentration of 15-LOX-1 was determined by an enzyme activity assay and proved to be a 40-fold dilution. The assay buffer consists of 25 mM *N*-(2-hydroxyethyl)piperazine-*N'*-ethanesulfonic acid titrated to pH 7.4. The substrate, linoleic acid (LA) (Sigma-Aldrich, L1376), was dissolved in ethanol to a concentration of 500 nM. The absorbance increased at 234 nm over time for the conversion of linoleic acid in the presence (positive control) of the enzyme or remained constant in the absence (blank control) of the enzyme.

To determine IC_{50} values, 140 μ L of the inhibitors (0–71 μ M, 2 \times dilution series) was incubated with 50 μ L of 1:40 enzyme solution for 10 min at room temperature in a 96-well plate. After 10 min incubation, 10 μ L of 500 nM LA was added to the mixture, which resulted in desired concentrations of the inhibitors (0–50 μ M, 2 \times dilution series), a final dilution of the enzyme of 1:160, and 25 nM LA. The linear absorbance increased in the absence of the inhibitor was set to 100%, whereas the absorbance increased in the absence of the enzyme was set to 0%. All experiments were performed at least in triplicate. The average values and their standard deviations were plotted. Data analysis was performed using Microsoft Excel professional plus 2013 and GraphPad Prism 5.01.

4.4. Cell Culture and MTS and RAW-Blue NF- κ B Reporter Gene Assays. RAW 264.7 murine macrophages were obtained from ATCC (Wesel, Germany) and cultured in Dulbecco's modified Eagle's medium + GlutaMAX (Gibco by Life Technologies, The Netherlands) supplemented with 10% (v/v) fetal bovine serum and 100 U/mL 1% penicillin/streptomycin (Gibco, The Netherlands) in a humidified 5% CO₂ atmosphere at 37 °C. RAW-Blue macrophages were obtained from InvivoGen (Toulouse, France) and cultured in the same conditions, with the addition of 200 μ g/mL Zeocin to the culture medium as reported by the manufacturer.

RAW 264.7 cells were seeded at 5000 cells per well in a 96-well plate 1 day prior to the experiment. Cells were treated with **9c** (**i472**) at 0.1, 1, 5, 10, and 50 μ M for 48 h. The cell viability of the treated cells was determined by adding 20 μ L of the CellTiter reagent to each well. After 2 h incubation with the CellTiter reagent at 37 °C, the absorbance at 490 nm was measured using a Synergy H1 plate reader.

RAW-Blue cells were seeded at 10×10^4 cells per well in a 96-well plate 1 day before the start of the experiment. Cells were treated with **9c** (**i472**) at 0.2, 1, and 5 μ M and stimulated with 10 ng/mL LPS (Sigma-Aldrich, The Netherlands) and 10 ng/mL IFN γ (Sigma-Aldrich, The Netherlands) for 24 h. The secreted embryonic alkaline phosphatase (SEAP) release was measured to monitor the NF- κ B levels using the QuantiBlue reagent (InvivoGen, Toulouse, France). After 2 h

incubation at 37 °C, the absorbance at 635–655 nm was measured using a Synergy H1 plate reader according to the manufacturer's instructions.

4.5. LPS-Induced Cell Death. RAW 264.7 cells were seeded at 5000 cells per well in a 96-well plate. The ability of rescue was tested with the treatment of **9c** (**i472**) at 0.2, 1, and 5 μ M or Zileuton at 5 μ M with 100 μ g/mL LPS for 48 h. The cell viability was determined by the MTS assay as described above.³

4.6. Gene Expression Analysis by Quantitative Reverse Transcription Polymerase Chain Reaction (PCR). Total RNA was isolated from RAW 264.7 cells using the SV total RNA isolation system (Promega, Leiden, The Netherlands) according to the protocol of the manufacturer. RNA integrity was determined by 28S/18S ratio detection on an agarose gel, which was consistently found to be intact. For gene expression analysis, RNA was reverse-transcribed using a reverse-transcription kit (Promega). Subsequently, 10 ng of cDNA was applied for each real-time PCR, which was performed on an ABI Prism 7900HT sequence detection system (Applied Biosystems, Nieuwerkerk a/d IJssel, The Netherlands). The primers for NF- κ B1 (Fw, 5'-GAAATTCCTGATCCAGACAAAAAC-3', Rv, 5'-ATCACTT-CAATGGCCTCTGTGTAG-3'), NF- κ B2 (Fw, 5'-CTGGTGGACACATACAGGAAGAC-3', Rv, 5'-ATAGGCACTGTCTTCTTT-CACCTC-3'), RelA (Fw, 5'-CTTCTCAGCCATGGTACCTCT-3', Rv, 5'-CAAGTCTTCATCAGCATCAAATG-3'), RelB (Fw, 5'-CTTTGCCTATGATCCTTCTGC-3', Rv, 5'-GAGTCCAGTGA-TAGGGGCTCT-3') and iNOS (Fw, 5'-TATCAGGAAGAAATG-CAGGAGAT-3', Rv, 5'-GAGCAGCTGAGTACCTCATT-3') were purchased from Sigma. For each sample, the real-time PCR reactions were performed in triplicate, and the averages of the obtained C_t values were used for further calculations. Gene expression levels were normalized to the expression of the reference gene glyceraldehyde-3-phosphate dehydrogenase (GAPDH), which was not influenced by the experimental conditions, resulting in the ΔC_t value. Gene expression levels were calculated by the comparative C_t method ($2^{-\Delta\Delta C_t}$).

4.7. Nitric Oxide (NO) Assay. The level of nitric oxide was measured in RAW 264.7 cells. Macrophage cells (2×10^6 per well) were seeded in six-well plates and incubated 24 h with or without 10 ng/mL LPS (Sigma, The Netherlands) and 10 ng/mL IFN γ (Sigma-Aldrich, The Netherlands) in the presence or absence of 5 μ M **9c** (**i472**). The nitric oxide level in each sample was quantified using the commercially available colorimetric nitric oxide assay kit (abcam, ab 65328, U.K.) following the manufacturer's instructions.

4.8. Lipid Peroxidation. RAW 264.7 cells were seeded into a six-well plate containing 10×10^6 cells per well. After overnight incubation, cells were treated with 10 ng/mL LPS (Sigma, The Netherlands) and 10 ng/mL IFN γ (Sigma, The Netherlands) for 24 h in the presence or absence of 5 μ M PD146176, Zileuton, or **9c** (**i472**), respectively. Cells without LPS/IFN γ treatment were taken as a control. Lipid peroxidation was detected by staining with BODIPY 581/591 C11 (Invitrogen, Karlsruhe, Germany) at a final concentration of 2 mM for 30 min at 37 °C. The shift in fluorescence from red to green was analyzed by fluorescence-activated cell sorting (FACS) using the Guava Easy Cite 6-2L system (Merck Millipore, Darmstadt, Germany) by excitation at 488 nm. At least three independent experiments were performed per condition.

■ ASSOCIATED CONTENT

📄 Supporting Information

The Supporting Information is available free of charge on the ACS Publications website at DOI: 10.1021/acs.jmedchem.9b00212.

Docking study with the preferred overlapped poses of compounds **9c**, **9f**, and **16** (Figure S1), the 2-mercaptoethanol reactivity assay (Figure S2), the LPS toxicity assay (Figure S3), the MTS assay of **9c** (**i472**) (Figure S4), the FACS of RAW 264.7 cells (Figure S5), and 1H and ^{13}C NMR spectral data (Figure S6) (PDF)

HPLC analysis (PDF)

Molecular formula strings (CSV)

AUTHOR INFORMATION

Corresponding Author

*E-mail: f.j.dekker@rug.nl. Phone: +31-50-3638030. Fax: +31-50-3637953.

ORCID

Ramon van der Vlag: 0000-0002-8796-2792

Frank J. Dekker: 0000-0001-7217-9300

Notes

The authors declare no competing financial interest.

ACKNOWLEDGMENTS

We acknowledge The Netherlands Organisation for Scientific Research (NWO) for providing VIDI grant (016.122.302 and 723.014.008) to F.J.D. and A.K.H.H., respectively. We would like to thank Bin Liu and Shanshan Song for helpful advice and discussion.

ABBREVIATIONS

NO, nitric oxide; 15-LOX-1, 15-lipoxygenase-1; NF- κ B, nuclear factor- κ B; LPS, lipopolysaccharides; iNOS, inducible nitric oxide synthase; ROS, reactive oxygen species; AA, arachidonic acid; LA, linoleic acid; SAR, structure–activity relationships; IFN γ , interferon γ ; EDCI, 1-ethyl-3-(3-dimethylaminopropyl)-carbodiimide; HOBt, N-hydroxybenzotriazole; IC₅₀ value, 50% inhibition concentration

REFERENCES

- Linkermann, A.; Stockwell, B. R.; Krautwald, S.; Anders, H. J. Regulated Cell Death and Inflammation: An Auto-Amplification Loop Causes Organ Failure. *Nat. Rev. Immunol.* **2014**, *14*, 759–767.
- Fan, E. K. Y.; Fan, J. Regulation of Alveolar Macrophage Death in Acute Lung Inflammation. *Respir. Res.* **2018**, *19*, No. 50.
- Kim, I. D.; Ha, B. J. Toxicology in Vitro Paeoniflorin Protects RAW 264. 7 Macrophages from LPS-Induced Cytotoxicity and Genotoxicity. *Toxicol. in Vitro* **2009**, *23*, 1014–1019.
- Lee, S. H.; Soyoolas, E.; Chanmugaml, P.; Hart, S.; Sun, W.; Zhong, H.; Liou, S.; Simmons, D.; Hwang, D. Selective Expression of Mitogen-Inducible Cyclooxygenase in Macrophages Stimulated with Lipopolysaccharide. *J. Biol. Chem.* **1992**, *267*, 25934–25938.
- Yamamoto, H.; Omelchenko, I.; Shi, X.; Nuttall, A. L. The Influence of NF- κ B Signal-Transduction Pathways on the Murine Inner Ear by Acoustic Overstimulation. *J. Neurosci. Res.* **2009**, *87*, 1832–1840.
- Lawrence, T. The Nuclear Factor NF- κ B Pathway in Inflammation. *Cold Spring Harbor Perspect. Biol.* **2009**, *1*, No. a001651.
- Feng, H.; Stockwell, B. R. Unsolved Mysteries: How Does Lipid Peroxidation Cause Ferroptosis? *PLoS Biol.* **2018**, *16*, No. e2006203.
- Natarajan, R.; Reddy, M. A.; Malik, K. U.; Fatima, S.; Khan, B. V. Signaling Mechanisms of Nuclear Factor- κ B-Mediated Activation of Inflammatory Genes by 13-Hydroperoxyoctadecadienoic Acid in Cultured Vascular Smooth Muscle Cells. *Arterioscler., Thromb., Vasc. Biol.* **2001**, *21*, 1408–1413.
- Mendes, K. L.; Lelis, D. F.; Santos, S. H. S. Nuclear Sirtuins and in Inflammatory Signaling Pathways. *Cytokine Growth Factor Rev.* **2017**, *38*, 98–105.
- Vallance, P.; Leiper, J. Blocking No Synthesis: How, Where and Why? *Nat. Rev. Drug Discovery* **2002**, *1*, 939–950.
- Blaise, G. A.; Gauvin, D.; Gangal, M.; Authier, S. Nitric Oxide, Cell Signaling and Cell Death. *Toxicology* **2005**, *208*, 177–192.
- Chandel, N. S.; Trzyna, W. C.; David, S.; Schumacker, P. T. Role of Oxidants in NF- κ B Activation and TNF- α Gene Transcription Induced by Hypoxia and Endotoxin. *J. Immunol.* **2000**, *165*, 1013–1021.

(13) Dennis, E. A.; Norris, P. C. Eicosanoid Storm in Infection and Inflammation. *Nat. Rev. Immunol.* **2015**, *15*, 511–523.

(14) Haeggström, J. Z.; Funk, C. D. Lipoxygenase and Leukotriene Pathways: Biochemistry, Biology, and Roles in Disease. *Chem. Rev.* **2011**, *111*, 5866–5896.

(15) Solomon, E. I.; Zhou, J.; Neese, F.; Pave, E. G. New Insights from Spectroscopy Relationships of Lipoxygenases into the Structure/Function. *Chem. Biol.* **1997**, *4*, 795–808.

(16) Ivanov, I.; Heydeck, D.; Hofheinz, K.; Roffeis, J.; O'Donnell, V. B.; Kuhn, H.; Walther, M. Molecular Enzymology of Lipoxygenases. *Arch. Biochem. Biophys.* **2010**, *503*, 161–174.

(17) Jiro, S.; Hitoshi, A.; Tadahiko, K.; Tamotsu, T.; Akikazu, H. Purification and Some Properties of Potato Tuber Lipoxygenase and Detection of Linoleic Acid Radical in the Enzyme Reaction. *Agric. Biol. Chem.* **1977**, *41*, 827–832.

(18) Dobrian, A. D.; Lieb, D. C.; Cole, B. K.; Taylor-Fishwick, D. A.; Chakrabarti, S. K.; Nadler, J. L. Functional and Pathological Roles of the 12- and 15-Lipoxygenases. *Prog. Lipid Res.* **2011**, *50*, 115–131.

(19) Feltenmark, S.; Gautam, N.; Brunnström, A.; Griffiths, W.; Backman, L.; Edenius, C.; Lindbom, L.; Björkholm, M.; Claesson, H. E. Eoxins are Proinflammatory Arachidonic Acid Metabolites Produced via the 15-Lipoxygenase-1 Pathway in Human Eosinophils and Mast Cells. *Proc. Natl. Acad. Sci. U.S.A.* **2008**, *105*, 680–685.

(20) Schnurr, K.; Belkner, J.; Ursini, F.; Schewe, T.; Kühn, H. The Selenoenzyme Phospholipid Hydroperoxide Glutathione Peroxidase Controls the Activity of the 15-Lipoxygenase with Complex Substrates and Preserves the Specificity of the Oxygenation Products. *J. Biol. Chem.* **1996**, *271*, 4653–4658.

(21) Buczynski, M. W.; Dumlaio, D. S.; Dennis, E. A. Thematic Review Series: Proteomics. An Integrated Omics Analysis of Eicosanoid Biology. *J. Lipid. Res.* **2009**, *50*, 1015–1038.

(22) Latz, E.; Xiao, T. S.; Stutz, A. Activation and Regulation of the Inflammasomes. *Nat. Rev. Immunol.* **2013**, *13*, 397–411.

(23) Quehenberger, O.; Dennis, E. A. The Human Plasma Lipidome. *N. Engl. J. Med.* **2011**, *365*, 1812–1823.

(24) Yang, W. S.; Stockwell, B. R. Ferroptosis: Death by Lipid Peroxidation. *Trends Cell Biol.* **2016**, *26*, 165–176.

(25) Shetty, R. S.; Lee, Y.; Liu, B.; Husain, A.; Joseph, R. W.; Lu, Y.; Nelson, D.; Mihelcic, J.; Chao, W.; Moffett, K. K.; Schumacher, A.; Flubacher, D.; Stojanovic, A.; Bukhtiyarova, M.; Williams, K.; Lee, K.; Ochman, A. R.; Saporito, M. S.; Moore, W. R.; Flynn, G. A.; Dorsey, B. D.; Springman, E. B.; Fujimoto, T.; Kelly, M. J. Synthesis and Pharmacological Evaluation of N-(3-(1H-Indol-4-Yl)-5-(2-Methoxyisonicotinoyl)phenyl)methanesulfonamide (LP-261), a Potent Antimitotic Agent. *J. Med. Chem.* **2011**, *54*, 179–200.

(26) Ivanov, I.; Kuhn, H.; Heydeck, D. Structural and Functional Biology of Arachidonic Acid 15-Lipoxygenase-1 (ALOX15). *Gene* **2015**, *573*, 1–32.

(27) Sendobry, S. M.; Cornicelli, J. A.; Welch, K.; Bocan, T.; Tait, B.; Trivedi, B. K.; Colbry, N.; Dyer, R. D.; Feinmark, S. J.; Daugherty, A. Attenuation of Diet-Induced Atherosclerosis in Rabbits with a Highly Selective 15-Lipoxygenase Inhibitor Lacking Significant Antioxidant Properties. *Br. J. Pharmacol.* **1997**, *120*, 1199–1206.

(28) Weinstein, D. S.; Liu, W.; Gu, Z.; Langevine, C.; Ngu, K.; Fadnis, L.; Combs, D. W.; Sitkoff, D.; Ahmad, S.; Zhuang, S.; Chen, X.; Wang, F. L.; Loughney, D. A.; Atwal, K. S.; Zahler, R.; Macor, J. E.; Madsen, C. S.; Murugesan, N. Tryptamine and Homotryptamine-Based Sulfonamides as Potent and Selective Inhibitors of 15-Lipoxygenase. *Bioorg. Med. Chem. Lett.* **2005**, *15*, 1435–1440.

(29) ElBordiny, H. S.; El-Miligy, M. M.; Kassab, S. E.; Daabees, H.; Mohamed, A. W.; Abdelhamid, M. E. S. Design, Synthesis, Biological Evaluation and Docking Studies of New Derivatives as Potent Antioxidants and 15-Lipoxygenase Inhibitors. *Eur. J. Med. Chem.* **2018**, *145*, 594–605.

(30) Eleftheriadis, N.; Neochoritis, C. G.; Leus, N. G. J.; Van Der Wouden, P. E.; Dömling, A.; Dekker, F. J. Rational Development of a Potent 15-Lipoxygenase-1 Inhibitor with in Vitro and Ex Vivo Anti-Inflammatory Properties. *J. Med. Chem.* **2015**, *58*, 7850–7862.

(31) Rai, G.; Joshi, N.; Jung, J. E.; Liu, Y.; Yasgar, A.; Simeonov, A.; Jadhav, A.; Perry, S.; Diaz, G.; Kenyon, V.; van Leyen, K.; Zhang, Q.; Schultz, L.; Lo, E.; Maloney, D. J.; Holman, T. R. Potent and Selective Inhibitors of Human Reticulocyte 12/15-Lipoxygenase as Anti-Stroke Therapies. *J. Med. Chem.* **2014**, *57*, 4035–4048.

(32) Bråthe, A.; Andresen, G.; Gundersen, L. L.; Malterud, K. E.; Rise, F. Antioxidant Activity of Synthetic Cytokinin Analogues: 6-Alkynyl- and 6-Alkenylpurines as Novel 15-Lipoxygenase Inhibitors. *Bioorg. Med. Chem.* **2002**, *10*, 1581–1586.

(33) Guo, H.; Eleftheriadis, N.; Rohr-udilova, N.; Alexander, D.; Dekker, F. J. Photoactivation Provides a Mechanistic Explanation for Pan-Assay Interference Behaviour of 2-Aminopyrroles in Lipoxygenase Inhibition. *Eur. J. Med. Chem.* **2017**, *139*, 633–643.

(34) Eleftheriadis, N.; Thee, S. A.; Zwinderman, M. R. H.; Leus, N. G. J.; Dekker, F. J. Activity-Based Probes for 15-Lipoxygenase-1. *Angew. Chem., Int. Ed.* **2016**, *55*, 12300–12305.

(35) Isobe, Y.; Kawashima, Y.; Ishihara, T.; Watanabe, K.; Ohara, O.; Arita, M. Identification of Protein Targets of 12/15-Lipoxygenase-Derived Lipid Electrophiles in Mouse Peritoneal Macrophages Using Omega-Alkynyl Fatty Acid. *ACS Chem. Biol.* **2018**, *13*, 887–893.

(36) Gore, V.; Patel, P.; Chang, C.; Sivendran, S.; Kang, N.; Ouedraogo, Y. P.; Gravel, S.; Powell, W. S.; Rokach, J. 5-Oxo-ETE Receptor Antagonists. *J. Med. Chem.* **2013**, *56*, 3725–3732.

(37) Bergelson, L. D.; Shemyakin, M. M. Synthesis of Naturally Occurring Unsaturated Fatty Acids by Sterically Controlled Carbonyl Olefination. *Angew. Chem., Int. Ed.* **1964**, *3*, 250–260.

(38) Eleftheriadis, N.; Poelman, H.; Leus, N. G. J.; Honrath, B.; Neochoritis, C. G.; Dolga, A.; Dömling, A.; Dekker, F. J. Design of a Novel Thiophene Inhibitor of 15-Lipoxygenase-1 with Both Anti-Inflammatory and Neuroprotective Properties. *Eur. J. Med. Chem.* **2016**, *122*, 786–801.

(39) Gillmor, S. A.; Villaseñor, A.; Fletterick, R.; Sigal, E.; Browner, M. F. The Structure of Mammalian 15-Lipoxygenase Reveals Similarity to the Lipases and the Determinants of Substrate Specificity. *Nat. Struct. Biol.* **1997**, *4*, 1003–1009.

(40) Ourailidou, M. E.; Dockerty, P.; Witte, M.; Poelarends, G. J.; Dekker, F. J. Metabolic Alkene Labeling and in Vitro Detection of Histone Acylation via the Aqueous Oxidative Heck Reaction. *Org. Biomol. Chem.* **2015**, *13*, 3648–3653.

(41) Jung, D. H.; Kim, K. H.; Byeon, H. E.; Park, H. J.; Park, B.; Rhee, D. K.; Um, S. H.; Pyo, S. Involvement of ATF3 in the Negative Regulation of iNOS Expression and NO Production in Activated Macrophages. *Immunol. Res.* **2015**, *62*, 35–45.

(42) Moncada, S.; Palmer, R. M.; Higgs, E. A. Nitric Oxide: Physiology, Pathophysiology, and Pharmacology. *Pharmacol. Rev.* **1991**, *43*, 109–142.

(43) Sies, H. On the History of Oxidative Stress: Concept and Some Aspects of Current Development. *Curr. Opin. Toxicol.* **2018**, *7*, 122–126.

(44) Naguib, Y. M. A Fluorometric Method for Measurement of Peroxyl Radical Scavenging Activities of Lipophilic Antioxidants. *Anal. Biochem.* **1998**, *298*, 290–298.

(45) Chen, H.; Yang, H.; Wang, Z.; Xie, X.; Nan, F. Discovery of 3-Substituted 1*H*-Indole-2-Carboxylic Acid Derivatives as a Novel Class of CysLT₁ Selective Antagonists. *ACS Med. Chem. Lett.* **2016**, *7*, 335–339.

(46) Eleftheriadis, N.; Thee, S.; te Biesebeek, J.; van der Wouden, P.; Baas, B. J.; Dekker, F. J. Identification of 6-Benzoyloxysalicylates as a Novel Class of Inhibitors of 15-Lipoxygenase-1. *Eur. J. Med. Chem.* **2015**, *94*, 265–275.